



BRAG2a Mediates mGluR-Dependent AMPA Receptor Internalization at Excitatory Postsynapses through the Interaction with PSD-95 and Endophilin 3

 Masahiro Fukaya,¹ Takeyuki Sugawara,¹ Yoshinobu Hara,¹ Makoto Itakura,²  Masahiko Watanabe,³ and Hiroyuki Sakagami¹

¹Department of Anatomy, Kitasato University School of Medicine, Sagamihara 252-0374, Japan, ²Department of Biochemistry, Kitasato University School of Medicine, Sagamihara 252-0374, Japan, and ³Department of Anatomy, Faculty of Medicine, Hokkaido University, Sapporo 060-8638, Japan

Brefeldin A-resistant ArfGEF 2 (BRAG2) [or Iqsec1 (IQ motif and Sec7 domain-containing protein 1)] is a guanine nucleotide exchange factor for ADP ribosylation factor 6 (Arf6), a small GTPase implicated in the membrane trafficking between the plasma membrane and endosomes. BRAG2 regulates Arf6-dependent endocytosis of AMPA receptors (AMPA receptors) through the direct interaction during the hippocampal long-term depression. However, the molecular mechanism by which the BRAG2–Arf6 pathway links AMPARs to the endocytic machinery remains elusive. Herein, using mouse brains of both sexes, we demonstrated that BRAG2a, an alternative isoform with a long C-terminal insert containing a proline-rich domain and type I PDZ-binding motif, was selectively localized to the excitatory postsynaptic density (PSD). Using yeast two-hybrid screening, we identified PSD-95 and endophilin 1/3 as BRAG2a-binding partners in the brain. The interaction with PSD-95 was required for synaptic targeting of BRAG2a. In cultured hippocampal neurons, stimulation of group I metabotropic glutamate receptors (mGluRs) increased the interaction of BRAG2a with endophilin 3 and concomitant Arf6 activation in a time-dependent manner. Knockdown of BRAG2 in cultured hippocampal neurons blocked the mGluR-dependent decrease in surface AMPAR levels, which was rescued by introducing wild-type BRAG2a, but not wild-type BRAG2b or BRAG2a mutants lacking the ability to activate Arf6 or to interact with endophilin 3 or PSD-95. Further postembedding immunoelectron microscopic analysis revealed the preorganized lateral distribution of BRAG2a, Arf6, and endophilin 3 for efficient endocytosis at the postsynaptic membrane. Together, the present findings unveiled a novel molecular mechanism by which BRAG2a links AMPARs to the clathrin-dependent endocytic pathway through its interaction with PSD-95 and endophilin 3.

Key words: AMPA receptor; Arf6; BRAG2; endophilin; PSD; synapse

Significance Statement

BRAG2/Iqsec1 is a GDP/GTP exchange factor for ADP ribosylation factor 6 (Arf6), a small GTPase implicated in the membrane trafficking between the plasma membrane and endosomes, and regulates Arf6-dependent endocytosis of AMPARs through direct interaction during hippocampal long-term depression, one of the mechanisms of synaptic plasticity related to learning and memory. However, the molecular mechanism by which the BRAG2–Arf6 pathway links AMPARs to the endocytic machinery remains elusive. Here, we identified isoform-specific mechanisms of BRAG2-mediated AMPAR internalization. We demonstrated that the interaction of BRAG2a isoform with PSD-95 and endophilin 3 was required for the mGluR-dependent decrease in surface AMPARs in hippocampal neurons. These results unveiled a novel molecular mechanism by which BRAG2 links AMPARs to the clathrin-mediated endocytic machinery at postsynaptic sites.

Received July 10, 2019; revised Nov. 6, 2019; accepted Apr. 17, 2020.

Author contributions: M.F. and H.S. designed research; M.F., T.S., and H.S. performed research; M.I. and M.W. contributed unpublished reagents/analytic tools; M.F. and Y.H. analyzed data; M.F. and H.S. wrote the paper.

This study was supported by Japan Society for the Promotion of Science KAKENHI Grants 20K07250 (H.S.) and 17K07082 (M.F.), and the Takeda Science Foundation (M.F.). We thank the staff of the Bio-Imaging Center at Kitasato University School of Medicine for technical support in electron microscopic analyses.

The authors declare no competing financial interests.

Correspondence should be addressed to Hiroyuki Sakagami at sakagami@med.kitasato-u.ac.jp.

<https://doi.org/10.1523/JNEUROSCI.1645-19.2020>

Copyright © 2020 the authors

Introduction

Dynamic changes in the number and subunit composition of AMPARs by membrane trafficking such as exocytosis and endocytosis is a major regulatory mechanism underlying activity-dependent synaptic plasticity such as long-term potentiation (LTP) and long-term depression (LTD), the cellular basis of learning and memory (Sheng and Lee, 2001; Malinow and Malenka, 2002; Diering and Huganir, 2018). Hippocampal LTD is a form of activity-dependent synaptic plasticity that shows a persistent

decrease in synaptic strength and relates to learning and memory that require behavioral flexibility, such as the acquisition of novel information (Collingridge et al., 2010). During the LTD induction, clathrin-mediated endocytosis (CME) is thought to be a critical process to reduce AMPARs at the postsynaptic membrane downstream of NMDAR or mGluR activation. Consistently, several components of the CME machinery, including adaptor protein complex-2 (AP-2), clathrin, endophilin, and dynamin, are implicated in AMPAR internalization during LTD (Carroll et al., 1999; Man et al., 2000; Lee et al., 2002; Chowdhury et al., 2006; Nadif Kasri et al., 2011). Among these, endophilins, a family of Bin/Amphiphysin/Rvs (BAR) domain and Src homology 3 (SH3) domain-containing proteins, mediate various steps of CME, including the budding, fission, and uncoating of clathrin-coated vesicles (Ringstad et al., 1997, 1999; Schuske et al., 2003). During hippocampal mGluR-dependent LTD, endophilin cooperates with dynamin and oligophrenin-1, a Rho-GTPase activating protein, to mediate AMPAR internalization (Nadif Kasri et al., 2011). Endophilin and dynamin also form a protein complex with Arc/Arg3.1, and facilitate the endocytosis of AMPARs during homeostatic synaptic scaling and LTD (Chowdhury et al., 2006; Shepherd et al., 2006). However, our understanding of the molecular mechanisms of LTD is still far from complete.

BRAG2 (Brefeldin A-resistant ArfGEF 2), also known as Iqsec1 (IQ motif and Sec7 domain-containing protein 1), is a guanine nucleotide exchange factor (GEF) that activates ADP ribosylation factor 6 (Arf6; Someya et al., 2001), a small GTPase that regulates endosomal trafficking between the plasma membrane and endosomes. Arf6 is implicated in various neuronal functions including neuronal migration (Falace et al., 2014; Hara et al., 2016); formation of axons, dendrites, and dendritic spines (Hernández-Deviez et al., 2002, 2004; Miyazaki et al., 2005; Choi et al., 2006; Kim et al., 2015); and recycling of synaptic vesicles at presynapses (Tagliatti et al., 2016). The BRAG2–Arf6 pathway has been highlighted as a novel regulatory mechanism for activity-dependent AMPAR endocytosis (Scholz et al., 2010). During mGluR-dependent LTD, concomitant ligand binding to AMPAR and dephosphorylation of the GluA2 subunit at Tyr876 triggers direct interaction of BRAG2 with GluA2 and Arf6 activation, thereby leading to AMPAR endocytosis. Although the BRAG2–Arf6 pathway has been shown to mediate both mGluR-dependent and NMDAR-dependent LTD at hippocampal synapses, the latter form of LTD does not depend on tyrosine dephosphorylation (Scholz et al., 2010). Therefore, there seem to be additional mechanisms by which the BRAG2–Arf6 pathway regulates AMPAR endocytosis. In addition, BRAG2 exists in at least two isoforms, BRAG2a and BRAG2b, which differ by the alternative use of N-terminal and C-terminal regions (D'Souza and Casanova, 2016). Particularly, BRAG2a is unique in that it has a long C-terminal region containing a proline-rich domain (PRD) and a type I postsynaptic density-95 (PSD-95)/Discs large/zonula occludens 1 (PDZ)-binding motif. However, it remains unknown whether these two BRAG2 isoforms exhibit distinct subcellular localization and functions in neurons.

Here, we demonstrated that BRAG2a was selectively localized to the excitatory PSD through the interaction with PSD-95. We further identified endophilin 3 as a novel BRAG2a binding partner and demonstrated that the interaction of BRAG2a with PSD-95 and endophilin 3 was required for the mGluR-dependent decrease in surface AMPARs in cultured hippocampal neurons. These results unveiled a novel molecular mechanism by which BRAG2 links AMPARs to the CME machinery.

Materials and Methods

Animals. Three male C57BL/6 mice in the 10th to 12th postnatal weeks (CLEA Japan) were used for each analysis, including *in situ* hybridization, immunostaining, immunoelectron microscopy, and immunoblotting assays, five male C57BL/6 mice in the fourth postnatal week (CLEA Japan) were used for acute hippocampal slice culture, 20 pregnant ICR mice (CLEA Japan) were used for hippocampal primary culture, and two guinea pigs and one rabbit (Japan Laboratory Animals) were used for immunization. All animals were housed in air-conditioned rooms (~23°C) with a 12 h light/dark cycle with free access to food and water. Before the experiments, all animals were anesthetized with sodium pentobarbital (50 mg/kg body weight, i.p.) or inhalation of 4% isoflurane, and the anesthetic levels were assessed by pedal reflex to minimize suffering of the animals. Neonatal mice were killed by decapitation for the hippocampal neuronal culture. All efforts were made to minimize the number of animals used. All experimental protocols involving animals were approved by the Animal Experimentation and Ethics Committee of the Kitasato University School of Medicine.

In situ hybridization. *In situ* hybridization analysis was performed using ³⁵S-labeled antisense oligonucleotide probes, as described previously (Sakagami et al., 2006). Probes specific for BRAG2a and BRAG2b are complementary to nucleotides 3265–3309 and 2844–2888 of the cDNAs for mouse BRAG2a (GenBank accession no. NM_001134384) and BRAG2b (GenBank accession no. NM_001134383), respectively. A probe common to BRAG2a and BRAG2b (panBRAG2 probe) is complementary to nucleotides 2710–2754 of BRAG2a. Oligonucleotides were labeled with [α -³⁵S]-dATP using Invitrogen terminal deoxyribonucleotidyl transferase (Thermo Fisher Scientific). Cryostat sections (20 μ m in thickness) of freshly frozen adult mouse brains were subjected to the following treatments at room temperature: fixation with 4% paraformaldehyde (PFA) for 10 min; 2 mg/ml glycine in PBS for 10 min; acetylation with 0.25% acetic anhydride in 0.1 M triethanolamine-HCl, pH 8.0, for 10 min; and prehybridization for 1 h in a hybridization buffer consisting of 50% formamide, 0.1 M sodium phosphate buffer (PB), 4 \times SSC: 0.15 M NaCl, 0.015 M sodium citrate, pH 7.4), 0.02% Ficoll, 0.02% polyvinylpyrrolidone, 0.02% bovine serum albumin, 1% sodium N-lauroyl sarcosinate (sarkosyl), 200 μ g/ml tRNA, 1 mM EDTA, and 10% dextran sulfate. Hybridization was performed at 50°C overnight in the hybridization buffer supplemented with 100 mM dithiothreitol and ³⁵S-labeled oligonucleotide probes (1 \times 10⁷ cpm/ml). The slides were washed three times at 55°C for 40 min in 0.1 \times SSC containing 0.1% sarkosyl. Sections were exposed to nuclear track emulsion (NTB-2, Kodak) for 1 month. The specificity of the signals was confirmed by blank signals obtained when sections were hybridized in the presence of a 50-fold excess of unlabeled oligonucleotides.

Constructs of plasmid vectors. The cDNAs for BRAG2a, BRAG2b, PSD-95, PSD-93, SAP97, SAP102, GluN2A, GluN2B, endophilin 3, Arf6, GluA2, and their various mutants were amplified from mouse brain cDNA library or respective mouse cDNAs by PCR using the combinations of primers shown in Table 1, in which sense and antisense primers were supplemented at their 5' ends with a restriction site and a stop codon, respectively, and subcloned into pGEM-Teasy vectors (Promega). The inserts were confirmed by sequencing and subcloned into Invitrogen pDBLeu or pPC86 vectors (Thermo Fisher Scientific) for yeast two-hybrid assay, pCAGGS-FLAG, pcDNA, pEGFP-C, pEGFP-N, or pmCherry-C vectors (Clontech Laboratories) for protein expression in mammalian cells, and pGEX4T-2 (GE Healthcare Bio-Sciences) for protein expression in bacteria. The shRNA-resistant (sh-res) wild-type (WT) BRAG2a, its mutants, in which the C-terminal PDZ binding motif or Sec7 domain were deleted (Δ STVV or Δ Sec7), or proline residues at 956–957, 988–990, or all of the PxxP motifs in the PRD for the interaction with SH3 domain were replaced with alanine [P956/957A, P988-990A, or P(PR)A], and shRNA-resistant wild-type BRAG2b were made by gene synthesis (Europhins Genomics). For knock-down (KD) experiments, target sequences (BRAG2, 5'-GT CGCATTGTGCTGTCCAA-3'; firefly luciferase for control, 5'-CGTAC GCGGAATACTTCGA-3') were subcloned into modified mU6pro vectors, which can simultaneously express shRNA under a U6 promoter and EGFP under a CMV promoter (Yazaki et al., 2014). Plasmids used

Table 1. PCR Primers used in the present study

Product name	Sense	Antisense
BRAG2a (1–1099)	GAATTCATGGCTGCCGAAGACGC	CTACACAACCTGTGCTGATGC
BRAG2a (934–1099)	GTCGACAGGCTCCATCATTAGCAGT	CTACACAACCTGTGCTGATGC
BRAG2a (934–1095)	GTCGACAGGCTCCATCATTAGCAGT	CTAGATGCCCTGGGCTTGGC
BRAG2a (934–1002)	GTCGACAGGCTCCATCATTAGCAGT	CTATTCTGAGGGCCAGGGTGAT
BRAG2a (1002–1095)	GTCGACAGAAGGCCCATGCTATGG	CTAGATGCCCTGGGCTTGGC
BRAG2a (1014–1089)	GGATCCCATGCACAGCAAGAATCCTCC	CTACTTGTCTGCTGGGGGGGCG
BRAG2b (1–961)	GGATCCATGTGGTGCCTGCATGCAA	CTAGGACACAGCACTGGAGGCTG
BRAG2b (948–961)	GGATCCGAATTCAGCCCTCCAGCC	CTAGGACACAGCACTGGAGGCTG
PSD-95 full	GTCGACCATGGACTGTCTGTATAGTGACAACC	TCAGAGTCTCTCTCGGGCTGGACCC
PSD-95 PDZ1 + 2 + 3	GTCGACCATGGAGTATGAGGAGATCACATTGG	TTACCGAAGATCATGGATCTTGG
PSD-95 PDZ1 + 2	GTCGACCATGGAGTATGAGGAGATCACATTGG	CTAGCTGTACTCAGGTAGGC
PSD-95 PDZ2 + 3	GTCGACCATCATAGAGATCAAGCTTATCAAAG	TTACCGAAGATCATGGATCTTGG
PSD-95 PDZ1	GTCGACCATGGAGTATGAGGAGATCACATTGG	CTAAGCTGGGGTTCCGGCCGATG
PSD-95 PDZ2	GTCGACCATCATAGAGATCAAGCTTATCAAAG	CTAGCTGTACTCAGGTAGGC
PSD-95 PDZ3	GTCGACCATGACCCCACTCCCTCGGCGC	TTACCGAAGATCATGGATCTTGG
Endophilin 3 (1–347)	GTCGACGATGTCGGTGGCTGGGCTC	TTACGGAGGTAAGGCAC
Endophilin 3 (1–249)	GTCGACGATGTCGGTGGCTGGGCTC	CTATGGATGCAAGAGATA
Endophilin 3 (250–347)	GTCGACAGTCCCCAAGCGAAGATTC	TTACGGAGGTAAGGCAC
Endophilin 3 (286–347)	GTCGACGACGACCCCTGCTGCTGT	TTACGGAGGTAAGGCAC
PSD-93 full	CTCGAGAATGTTCTTTCATGTTATTGTGC	TTATAACTTCTCTTTGAGGGAATC
SAP97 full	GTCGACAATGCCGCTCCGGAAGCAAGATAC	TCATAGCTTTTCTTTCCTGGGACC
SAP102 full	GTCGACCATGCACAAGCACCAGCACTGCTG	TCAGAGTTTTTTCAGGGATGGGAC
GluN2A-CT (1038–1237)	GTCGACGACTGCAGAGAATAGGCCACTC	GCAATCACACTGAAAGGAGATCTCATGG
GluN2B-CT (1036–1243)	GTCGACGACGACTGTACGGCAAGTTCTC	TCACTCACACTGTGACGGCCTCGGGCC
GluA2 full	GTCGACATGCAAAAGATTATGCATAT	CTAAATTTAACACTCTCGA

for neuronal transfection were purified using the EndoFree Plasmid Maxi kit (Qiagen).

Yeast two-hybrid screening. To isolate BRAG2a-interacting proteins, we performed yeast two-hybrid screening using the Invitrogen ProQuest Two-Hybrid system (Thermo Fisher Scientific). The yeast two-hybrid method was previously described in detail (Fukaya et al., 2011). The Invitrogen MaV203 yeast cells (Thermo Fisher Scientific) were cotransformed with pDBLeu-BRAG2a (934–1099) and pPC86 prey vectors carrying the mouse brain cDNA library. A total of $\sim 4 \times 10^6$ transformants was subjected to auxotrophic selection on synthetic dropout medium lacking tryptophan, leucine, or histidine in the presence of 10 mM 3-amino-1,2,4-triazole. Positive colonies were further selected by the β -galactosidase activity and prototrophy for uracil in accordance with the manufacturer protocol. Candidate prey vectors were isolated and sequenced.

HeLa cells and transfection. HeLa cells, a cell line that had not been listed as a misidentified cell line by the International Cell Line Authentication Committee, were obtained from the Cell Resource Center for Biomedical Research (Tohoku University, Sendai, Japan) and maintained in DMEM supplemented with 10% fetal bovine serum in 5% CO₂ at 37°C. Cells were plated onto 35 mm dishes at a density of 0.2×10^6 per dish for immunostaining or 1.0×10^6 per dish for other analyses, and transfected with expression vectors using Invitrogen Lipofectamine 2000 (Thermo Fisher Scientific). One day after the transfection, cells were harvested and subjected to immunostaining, immunoblotting, pull-down assay, or immunoprecipitation analyses.

Antibodies. The antibodies used in this study are summarized in Table 2. To produce a specific antibody for BRAG2b, the C-terminal region (amino acids 948–961) of mouse BRAG2b was expressed as a fusion protein of glutathione S-transferase (GST) in Rosetta (DE3)pLysS cells (catalog #70956-3CN, Novagen) transformed with pGEX-4T-2-BRAG2b (948–961) in the presence of 0.1 mM isopropyl- β -D-thiogalactopyranoside at 25°C overnight, and purified using glutathione-Sepharose 4B (GE Healthcare). The GST fusion protein was emulsified with Freund's adjuvant and injected subcutaneously into a rabbit five times at 2-week intervals. After the antibody against GST was subtracted from the serum using GST-coupled Sepharose 4B beads (GE Healthcare), the specific antibody was affinity-purified using GST-BRAG2b (948–961)-Sepharose 4B beads. The guinea pig anti-BRAG2a antibody

was produced using the C-terminal region (amino acids 1014–1089) of BRAG2a (Sakagami et al., 2017).

Immunostaining for brain sections. Under deep anesthesia with sodium pentobarbital (50 mg/kg body weight, i.p.), mice were transcardially perfused with 4% PFA in 0.1 M PB for immunoperoxidase and immunofluorescence, or 4% PFA/0.1% glutaraldehyde in 0.1 M PB for postembedding immunoelectron microscopy. Brains were postfixed with the same fixative for 3 h. Floating sections were made at a thickness of 50 μ m on a vibrating microtome (VT1000, Leica) and treated with 1 mg/ml pepsin in 0.2N HCl solution for 5 min at 37°C for antigen retrieval (Fukaya and Watanabe, 2000). For immunoperoxidase, sections were incubated with 5% donkey serum in PBS, followed by incubation with primary antibody against BRAG2a (0.5 μ g/ml, guinea pig) or BRAG2b (1.0 μ g/ml, rabbit) overnight, with biotinylated secondary antibody (1:200; catalog #BA-7000, Vector Laboratories) for 2 h, and then with the avidin–biotin–peroxidase complex (DAKO) for 1 h. The immunoreaction was visualized in substrate solution containing 3,3'-diaminobenzidine and hydrogen peroxide (catalog #GV825, DAKO). For immunofluorescence, floating sections were incubated with the following combinations of primary antibodies: anti-BRAG2a antibody (0.5 μ g/ml, guinea pig) and antibodies against BRAG2b (1.0 μ g/ml, rabbit), PSD-95 (0.5 μ g/ml, rabbit), panAMPA (0.5 μ g/ml, goat), VGluT1 (0.5 μ g/ml, rabbit), or BRAG3 (0.5 μ g/ml, rabbit), and anti-BRAG2b antibody (1.0 μ g/ml, rabbit) and anti-PSD-95 antibody (0.5 μ g/ml, guinea pig), MAP2 (0.5 μ g/ml, goat), or EEA1 (0.5 μ g/ml, mouse). The immunoreaction was visualized using species-specific secondary antibodies conjugated with Alexa Fluor 488 or Alexa Fluor 594 (0.5 μ g/ml for each; A-21206, A-21202, Invitrogen; 705–545-147, 705–585-147, Jackson ImmunoResearch). Sections were counterstained with 4',6-diamidino-2-phenylindole dihydrochloride (DAPI; catalog #10236276001, Roche) and examined using a confocal laser microscope (model LSM 710, Carl Zeiss). Postembedding immunoelectron microscopy was performed as described previously (Fukaya et al., 2003) with minor modifications. Microslicer sections of the hippocampal formation (400 μ m in thickness) were cryoprotected with 30% sucrose in 0.1 M PB and frozen rapidly with liquid propane in a Leica EM CPC unit. Frozen sections were immersed in 0.5% uranyl acetate in methanol at -90°C in a Leica AFS freeze-substitution unit, infiltrated at -45°C with Lowicryl HM-20 resin (Lowi) and polymerized with UV light. After etching with saturated

Table 2. Antibodies used in the present study

Antibody	Immunogen	Species and dilution	Source
BRAG2a	Recombinant protein corresponding to the 76 aa (1014–1089) of mouse BRAG2a	GP and Rb polyclonal, 0.5 μ g/ml (IB, IHC, IF, IEM)	GP: this study Rb: Sakagami et al., 2017 RRID: AB_2827673
BRAG2b	Recombinant protein corresponding to the amino acids (948–961) of mouse BRAG2b	Rb polyclonal, 1 μ g/ml (IB, IHC, IF)	This study RRID: AB_2827674
panBRAG2	Recombinant protein corresponding to the amino acids (259–366) of mouse BRAG2b	GP polyclonal, 0.5 μ g/ml (IB, IF)	Sakagami et al., 2013 RRID: AB_2819239
BRAG1	Recombinant protein corresponding to the 116 aa (1364–1479) of mouse BRAG1	Rb polyclonal, 0.5 μ g/ml (IB)	Sakagami et al., 2008 RRID: AB_2314016
BRAG3	Recombinant protein corresponding to the 293 aa (1–293) of rat BRAG3	Rb polyclonal, 0.5 μ g/ml (IF)	Fukaya et al., 2011 RRID: AB_2827676
Arf6	Synthetic peptide corresponding to the 10 aa (166–175) of mouse Arf6	GP and Rb polyclonal, 0.5 μ g/ml (IB, IF, IEM)	Hara et al., 2016 RRID: AB_2819241
PSD-95	Recombinant protein corresponding to the N-terminal 64 aa (1–64) of mouse PSD-95	Rb polyclonal, 0.5 μ g/ml (IB, IF, IEM)	Frontier Institute, PSD-95-Rb-Af628; RRID: AB_2571540
SAP97	Recombinant protein corresponding to the 229 aa (1–229) of human SAP97	Mouse monoclonal, 0.5 μ g/ml (IB)	Santa Cruz Biotechnology, sc-9961, 2D11; RRID: AB_2092015
Endophilin 3	Synthetic peptide corresponding to the mouse endophilin 3	Goat polyclonal, 0.5 μ g/ml (IB, IF, IEM)	Santa Cruz Biotechnology, sc-10879, K-17; RRID: AB_2187420
panAMPA	Recombinant protein corresponding to the 19 aa (727–745) of mouse GluA1	GP polyclonal, 0.5 μ g/ml (IF)	Frontier Institute, panAMPA-GP; RRID: AB_2571610
GluA1	Recombinant protein corresponding to the 67 aa (841–907) of mouse GluA1	Rb polyclonal, 0.5 μ g/ml (IB, IF, IEM)	Frontier Institute, GluA1-Rb-Af690; RRID: AB_2571752
GluA2	Synthetic peptide corresponding to the 17 aa (847–863) of mouse GluA2	Rb polyclonal, 0.5 μ g/ml (IB, IF, IEM)	Frontier Institute, GluR2C-Rb-Af1050; RRID: AB_2571754
GluA1 (extracellular)	Synthetic peptide corresponding to the 15 aa (271–285) of mouse GluA1	Rb polyclonal, 1.0 μ g/ml (IF)	Alomone Labs, AGC-004; RRID: AB_2039878
Phospho-GluA2 (Tyr876)	Synthetic phosphopeptide corresponding to residues around pTyr876 of human GluA2	Rb polyclonal, 1:250 (IB)	Thermo Fisher Scientific, PA5-17096; RRID: AB_10982287
GluN2B (extracellular)	Recombinant protein corresponding to the 16 aa (27–42) of mouse GluN2B	Rb polyclonal, 1.0 μ g/ml (IF)	Watanabe et al., 1998 RRID: AB_2827677
VGLUT1	Recombinant protein corresponding to the C-terminal 30 aa (531–560) of mouse VGLUT1	Goat polyclonal, 0.5 μ g/ml (IF)	Frontier Institute, VGLUT1-Go-Af310; RRID: AB_2571617
EEA1	Recombinant protein corresponding to the amino acids (3–281) of human EEA1	Mouse monoclonal, 0.5 μ g/ml (IF)	BD Biosciences, 610457; RRID: AB_397830
MAP2	Recombinant protein corresponding to the 214 aa (927–1140) of mouse MAP2	Goat polyclonal, 0.5 μ g/ml (IF)	Frontier Institute, MAP2-Go-Af860; RRID: AB_2571557
Arc/Arg3.1	Recombinant protein corresponding to the 300 aa (1–300) of human Arc	Mouse monoclonal, 0.5 μ g/ml (IB)	Santa Cruz Biotechnology, sc-17839, C-7; RRID: AB_626696
AP-2 (α -adaptin)	Recombinant protein corresponding to the 178 aa (38–215) of mouse α -adaptin	Mouse monoclonal, 2.0 μ g/ml (IEM)	BD Transduction, 610501; RRID: AB_397867
Clathrin	Synthetic peptide corresponding to the 15 aa (1650–1664) of human clathrin heavy chain	Rb polyclonal, 2.0 μ g/ml (IEM)	Abcam, ab21679; RRID: AB_2083165
p38 MAPK	Synthetic peptide corresponding to the human p38 MAPK	Rb polyclonal, 1:500 (IB)	Cell Signaling Technology, #9212; RRID: AB_330713
Phospho-p38 MAPK	Synthetic phosphopeptide corresponding to residues around pThr180/pTyr182 of human p38 MAPK	Rb polyclonal, 1:500 (IB)	Cell Signaling Technology, #9211; RRID: AB_331641
α -Tubulin	Recombinant protein corresponding to the C-terminal 5 aa (426–430) of α -tubulin	Mouse monoclonal, 0.02 μ g/ml (IB)	Sigma-Aldrich, T9026 #DM1A; RRID: AB_477593
FLAG	Synthetic peptide: DYKDDDDK (FLAG-tag)	Mouse monoclonal, 0.1 μ g/ml (IB, IF)	Sigma-Aldrich, F1804; RRID: AB_262044
EGFP	Recombinant protein corresponding to the full-length EGFP	GP and Rb polyclonal, 0.2 μ g/ml (IF)	Sakagami et al., 2005 RRID: AB_2827678
mCherry	Recombinant protein corresponding to the full-length mCherry	GP polyclonal, 0.2 μ g/ml (IF)	Hara et al., 2013 RRID: AB_2827679

IEM, Immunoelectron microscopy; IF, immunofluorescence; IHC, immunohistochemistry; IB, immunoblotting; GP, guinea pig; Rb, rabbit.

sodium-ethanolate solution for 3 s, ultrathin sections on nickel grids were treated successively with 1% human serum albumin (Wako)/0.1% Tween 20 in Tris-buffered saline (HTBST), pH 7.5, for 1 h, primary antibodies (5 μ g/ml for each) in HTBST overnight, and colloidal gold (10 nm or 15 nm)-conjugated species-specific antibodies (1:100; British Bio Cell International) in HTBST for 2 h. Finally, sections were stained with 2% uranyl acetate solution for 15 min and 1% lead citrate solution for 1 min, and examined using an electron microscope (model H-7650, Hitachi). For quantitative analysis, perpendicular distribution of BRAG2a and lateral distribution of BRAG2a, PSD-95, GluA1/2, Arf6, endophilin 3, α -adaptin, and clathrin at axospinous synapses in the hippocampal CA1 pyramidal cells were evaluated by measurement of the length from the center

of gold particles to postsynaptic membrane and the edge of PSD, respectively, on electron microscopic images using ImageJ software (NIH).

Immunoprecipitation. HeLa cells were transfected with pCAGGS-FLAG-endophilin 3 and pCAGGS-FLAG-BRAG2a, pCAGGS-FLAG-BRAG2b, pCAGGS-FLAG-BRAG2a-P(PRND)A or pCAGGS-FLAG-BRAG2a-P956/957A, or pcDNA-GluA2 and pCAGGS-FLAG-BRAG2a, or pCAGGS-FLAG-BRAG2a- Δ Sec7 using Invitrogen Lipofectamine 2000 (Thermo Fisher Scientific). The cells were harvested with a buffer consisting of 50 mM Tris-HCl, pH 7.5, 150 mM NaCl, 1 mM EDTA, 1% Triton X-100, and a cocktail of protease inhibitors (catalog #11697498001, Roche). The lysates were immunoprecipitated with anti-endophilin 3 IgG- or anti-panBRAG2 IgG-conjugated magnetic beads

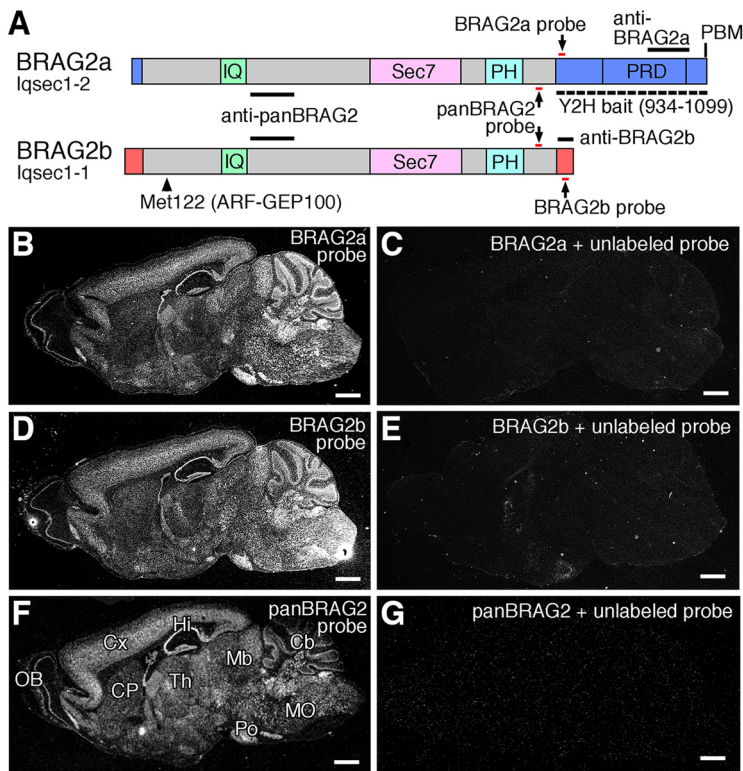


Figure 1. Domain structure and expression pattern of BRAG2. **A**, Schematic illustration of the domain structure of BRAG2a and BRAG2b isoforms. Black bars indicate antigen regions for common (panBRAG2), BRAG2a-specific, and BRAG2b-specific antibodies. Red bars pointed by arrows indicate common and isoform-specific oligonucleotide probe regions for *in situ* hybridization. An arrowhead indicates the methionine residue at position 122 of mouse BRAG2b, which is equivalent to an N-terminal residue of human ARF-GEP100. The dotted line indicates the BRAG2a-specific region used as bait for the yeast two-hybrid (Y2H) screening. IQ, Regulatory IQ-like motif; PBM, PDZ-binding motif; PH, pleckstrin homology domain; PRD, proline-rich domain; Sec7, catalytic Sec7 domain. **B–G**, *In situ* hybridization of the adult mouse brain using BRAG2a-specific (**B**, **C**), BRAG2b-specific (**D**, **E**), and panBRAG2 (**F**, **G**) probes. **C**, **E**, **G**, Negative control experiments were conducted by hybridizing adjacent sections with ^{35}S -labeled probes in the presence of excess amounts of the respective unlabeled probes. Note the indistinguishable expression patterns of BRAG2a, BRAG2b, and panBRAG2 probes. Cb, Cerebellum; CP, caudate putamen; Cx, cerebral cortex; Hi, hippocampus; OB, olfactory bulb; Mb, midbrain; MO, medulla oblongata; Po, pontine nuclei; Th, thalamus. Scale bars, 1 mm.

(Dynabeads, catalog #DB10004, Thermo Fisher Scientific). The immunoprecipitates and lysates were subjected to immunoblotting with anti-FLAG antibody (0.1 $\mu\text{g}/\text{ml}$) or anti-GluA2 antibody (0.5 $\mu\text{g}/\text{ml}$). For immunoprecipitation of the endogenous protein complex, whole mouse brains or cultured hippocampal neurons were homogenized in a buffer consisting of 10 mM Tris-HCl, pH 7.4, 320 mM sucrose, 10 mM EDTA, 10 mM EGTA, and protease inhibitors. After the nuclear and mitochondrial fractions were removed, the samples (P2 fraction, 200 μg) were dialyzed against a binding buffer consisting of 50 mM Tris-HCl, pH 7.4, and 1% Triton X-100 for 1 h at 4°C, and immunoprecipitated with anti-endophilin 3, PSD-95, BRAG2a, BRAG2b, or BRAG1 IgG-conjugated dynabeads. The immunoprecipitates were washed extensively with the binding buffer. The immunoprecipitates and lysates were subjected to immunoblotting with antibodies against BRAG2a, BRAG2b, BRAG1, PSD-95, endophilin 3, or GluA2. Immunoreactive bands were visualized using a chemiluminescent reagent (ECL-PLUS Western Blotting Detection Kit, Thermo Fisher Scientific) and quantified using an imaging analyzer (model LAS4000, GE Healthcare).

Arf6 pull-down assay. The GEF activity of BRAG2 was examined by an Arf6 pull-down assay with GGA3 (Arf6 activation assay kit, Cell Biolabs). Cultured hippocampal neurons treated with the group I mGluR agonist 3,5-dihydroxyphenylglycine (DHPG; Sigma-Aldrich) or HeLa cells transfected with pCAGGS-Arf6-FLAG (Hara et al., 2016), pCAGGS-FLAG-BRAG2a, and pCAGGS-FLAG-endophilin 3; pCAGGS-Arf6-FLAG and pCAGGS-FLAG-BRAG2a; or pCAGGS-FLAG-BRAG2a-

ΔSec7 were lysed in a buffer containing 25 mM HEPES, pH 7.5, 125 mM NaCl, 10 mM MgCl_2 , 1% NP-40, 1 mM EDTA, and 2% glycerol. After centrifugation, the supernatants were incubated with GGA3 agarose beads for 1 h at 4°C. The precipitates and lysates were subjected to immunoblotting with anti-Arf6, anti-BRAG2a, or anti-FLAG antibodies.

Hippocampal primary culture and treatment with agonists of glutamate receptors. The hippocampal neuronal culture was prepared as described previously (Beaudoin et al., 2012) with minor modifications. Hippocampi were dissected from neonatal mice (postnatal day 0), dissociated by trypsin treatment, and triturated through a Pasteur pipette in the plating medium. Hippocampal cells were seeded onto 35 mm dishes containing a thin plastic sheet (catalog #MS-92302Z, Cell Desk LF2, Sumitomo Bakelite) coated with poly-D-lysine (density, 1.2×10^6 cells/dish; Merck Millipore). Six hours after seeding, the plating medium was exchanged for the maintenance medium supplemented with B27 (Thermo Fisher Scientific). For immunoprecipitation assays, cultured neurons at 15 or 16 d *in vitro* (DIV15 or DIV16) were treated with the conditioned medium containing 0.1 μM tetrodotoxin (TTX; Sigma-Aldrich) for 30 min, followed by incubation with 50 μM phenylarsine oxide (PAO; tyrosine phosphatase inhibitor, Sigma-Aldrich) for 15 min, 100 μM NMDA (Sigma-Aldrich) for 5 min or 10 μM AMPA (Sigma-Aldrich) for 5 min in the conditioned medium. Neurons were harvested at 15, 30, and 60 min after each agonist treatment was initiated and subjected to immunoprecipitation or Arf6 pull-down assays. For cell surface AMPAR and NMDAR expression assays, cultured hippocampal neurons were transfected with shRNA vector for BRAG2 or luciferase (control) and pCAGGS-FLAG vector encoding shRNA-resistant wild-type BRAG2a, wild-type BRAG2b, BRAG2a-P956/957A, BRAG2a- ΔSTVV , or BRAG2a- ΔSec7 using Invitrogen Lipofectamine 3000 (Thermo Fisher Scientific) at DIV13 or DIV14. Two days after the transfection, neurons were treated with the conditioned medium containing 0.1 μM TTX for 30 min, followed by incubation with 50 μM DHPG for 15 min and the conditioned medium for 45 min. To label surface AMPA and NMDA receptors, cultured neurons were incubated with either GluA1 (extracellular) antibody (1.0 $\mu\text{g}/\text{ml}$; Alomone Labs) or GluN2B (extracellular) antibody (1.0 $\mu\text{g}/\text{ml}$; Watanabe et al., 1998) at 10°C for 30 min, washed quickly with warmed neuronal maintenance medium, and then subjected to immunostaining. For spine/dendrite localization assays, cultured neurons were transfected with pmCherry and pEGFP encoding wild-type BRAG2a, BRAG2a- ΔSTVV , wild-type BRAG2b, PSD-95, BRAG2a-P956/957A, or BRAG2a- ΔSec7 using Lipofectamine 3000 at DIV13 or DIV14. Two days after the transfection, neurons were fixed with 4% PFA in 0.1 M PB, pH 7.2, for 15 min, and the fluorescence for mCherry and EGFP was examined using a confocal laser microscope (model LSM 710, Carl Zeiss).

Immunostaining for cultured cells. For characterization of BRAG2 antibodies, 1 d after transfection HeLa cells were fixed with 4% PFA in 0.1 M PB, pH 7.2 at 25°C for 15 min, followed by permeabilization with 0.3% Triton X-100 in PBS for 30 min and blocking with 5% normal donkey serum in PBS for 30 min. Cells were incubated with antibodies against FLAG (mouse) and BRAG2a (guinea pig), BRAG2b (rabbit), or panBRAG2 (guinea pig). The immunoreaction was visualized using Alexa Fluor 488-conjugated donkey anti-mouse IgG (0.5 $\mu\text{g}/\text{ml}$; catalog

#A21202, Thermo Fisher Scientific) and Alexa Fluor 594-conjugated donkey anti-rabbit or guinea pig IgG (0.5 $\mu\text{g}/\text{ml}$; catalog #A32754, Thermo Fisher Scientific; catalog #706–515-148, Jackson ImmunoResearch). Cells were counterstained with DAPI (Roche). For characterization of shRNA for BRAG2, 2 d after transfection cultured hippocampal neurons were subjected to the same fixation, permeabilization, and blocking procedures as described above. Cells were subsequently incubated with anti-panBRAG2 (guinea pig) and anti-EGFP (rabbit) antibodies. The immunoreaction was visualized using Alexa Fluor 488-conjugated donkey anti-rabbit IgG (0.5 $\mu\text{g}/\text{ml}$; catalog #A32790, Thermo Fisher Scientific) and Alexa Fluor 594-conjugated donkey guinea pig IgG (0.5 $\mu\text{g}/\text{ml}$; catalog #706-515-148, Jackson ImmunoResearch). For cell surface AMPAR and NMDAR expression assays, cultured hippocampal neurons were incubated with either GluA1 (extracellular, rabbit) or GluN2B (extracellular, rabbit) antibody at 10°C for 30 min, and then fixed with 4% PFA in 0.1 M PB, pH 7.2, at 37°C for 15 min. After blocking with 2.5% normal donkey serum in PBS for 30 min, cells were incubated with anti-EGFP (guinea pig) antibody. The immunoreaction was visualized using Alexa Fluor 488-conjugated donkey anti-guinea pig IgG (0.5 $\mu\text{g}/\text{ml}$; catalog #706–545-148, Jackson ImmunoResearch) and Alexa Fluor 594-conjugated donkey anti-rabbit IgG (0.5 $\mu\text{g}/\text{ml}$; catalog #A32754, Thermo Fisher Scientific). Fluorescence signals were examined using a confocal laser microscope (model LSM 710, Carl Zeiss). Average fluorescence values for extracellular GluA1 and GluN2B were blindly measured on images, which were randomly selected by EGFP fluorescence, using ImageJ software (NIH). The background noise of extracellular GluA1 and GluN2B was negligible.

Acute hippocampal slice culture and DHPG treatment. Transverse hippocampal slices (300 μm in thickness) were prepared from 4-week-old C57BL/6 mice using a vibrating microtome equipped with an ice-cold chamber (model VT1200S, Leica) and incubated at 25°C for 1 h with artificial CSF (ACSF; 125 mM NaCl, 25 mM NaHCO_3 , 2.5 mM KCl, 1.25 mM NaH_2PO_4 , 1 mM MgCl_2 , 25 mM glucose, 10 mM bicuculline, and 0.1 μM TTX) bubbled with 95% O_2 /5% CO_2 . To induce mGluR-dependent chemical LTD, slices were treated with 50 μM DHPG in ACSF for 15 min and incubated with ACSF for 45 min. The slices were then fixed with 4% PFA/0.1% glutaraldehyde in 0.1 M PB for 15 min and subjected to postembedding immunoelectron microscopic analysis for synaptic and extrasynaptic localization of BRAG2a, PSD-95, and GluA1/2 at axospinous excitatory synapses in the stratum radiatum of CA1 region. Some slices were solubilized with the lysis buffer containing 50 mM Tris-HCl, pH 7.5, 150 mM NaCl, 1 mM EDTA, 1% Triton X-100, 1 mM Na_3VO_4 , 20 mM NaF, and protease inhibitor cocktail, and subjected to immunoblotting analysis with antibodies against GluA1/2, Arc/Arf3.1, phospho-p38, total p38, and α -tubulin.

Statistical analysis. For quantitative comparison, Student's *t* test was used for comparisons between the two evaluations within each group. Statistical significance was set at $p < 0.05$. For multiple comparisons, data were processed by the one-factor ANOVA with Tukey–Kramer

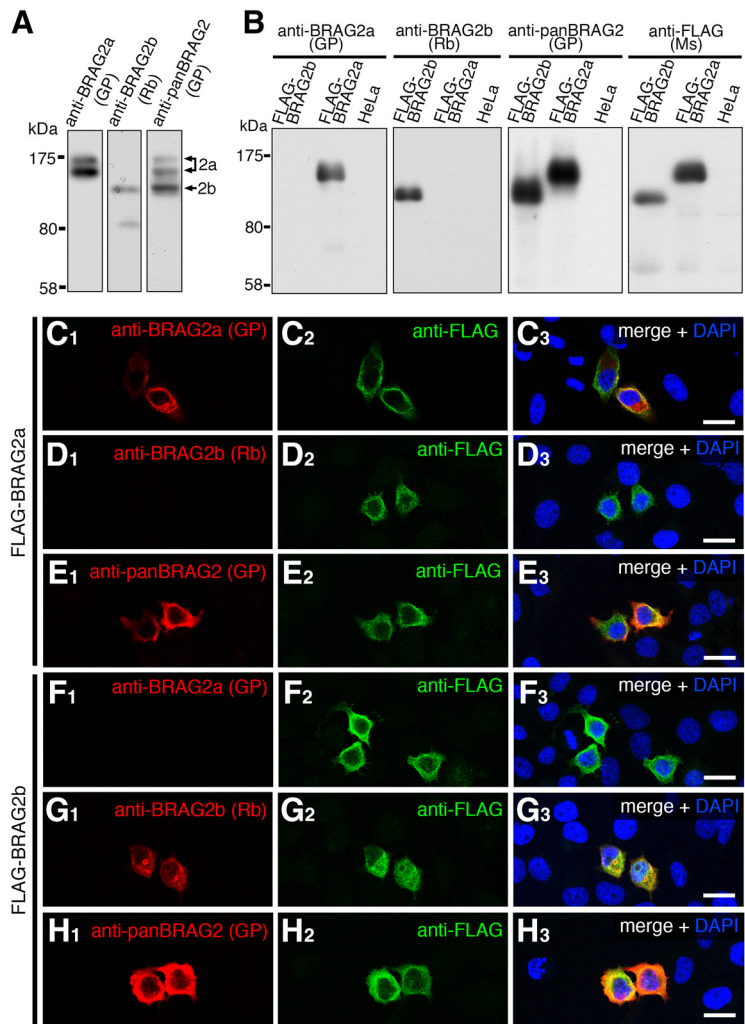


Figure 2. Characterization of BRAG2 antibodies. **A**, Immunoblotting of mouse brain lysates using guinea pig (GP) anti-BRAG2a, rabbit (Rb) anti-BRAG2b, and GP anti-panBRAG2 antibodies. Note that anti-panBRAG2, anti-BRAG2a, and anti-BRAG2b antibodies recognize three bands (160, 140, and 110 kDa), two bands (160 and 140 kDa), and a single band (110 kDa), respectively. **B**, Immunoblotting of HeLa cells transfected with FLAG-BRAG2a or FLAG-BRAG2b using anti-BRAG2a, anti-BRAG2b, anti-panBRAG2, and mouse (Ms) anti-FLAG antibodies. Note the specificity of anti-BRAG2a and anti-BRAG2b antibodies without cross-reactivity with FLAG-BRAG2b and FLAG-BRAG2a, respectively. **C–H**, Double immunofluorescence of HeLa cells transfected with FLAG-BRAG2a (**C–E**) or FLAG-BRAG2b (**F–H**) using anti-FLAG (**C₂–H₂**) and anti-BRAG2a (**C₁, F₁**), anti-BRAG2b (**D₁, G₁**), or anti-panBRAG2 (**E₁, H₁**) antibodies. Note the absence of the cross-reactivity of anti-BRAG2a and anti-BRAG2b antibodies with FLAG-BRAG2b and FLAG-BRAG2a, respectively. HeLa cells were counterstained with DAPI. Scale bars, 10 μm .

post hoc test. Data are presented as the mean \pm SD. Statistical analyses were performed using the StatView software 5.0 (SAS Institute).

Results

BRAG2a is enriched in excitatory postsynaptic density

The mouse *BRAG2/Iqsec1* gene generates at least two alternative splicing isoforms, BRAG2a/Iqsec1-2 and BRAG2b/Iqsec1-1, which differ in both the N-terminal and C-terminal regions (Fig. 1A). *In situ* hybridization analysis using ^{35}S -labeled isoform-specific and common oligonucleotide probes revealed that both BRAG2 isoforms exhibited indistinguishable patterns in the adult mouse brain with prominent expression in the cerebral cortex, hippocampus, cerebellar cortex, pontine nuclei, and various nuclei in the medulla oblongata (Fig. 1B,D,F). These hybridization signals were completely attenuated when 50-fold excess unlabeled oligonucleotides were included in the hybridization buffer (Fig. 1C,E,G).

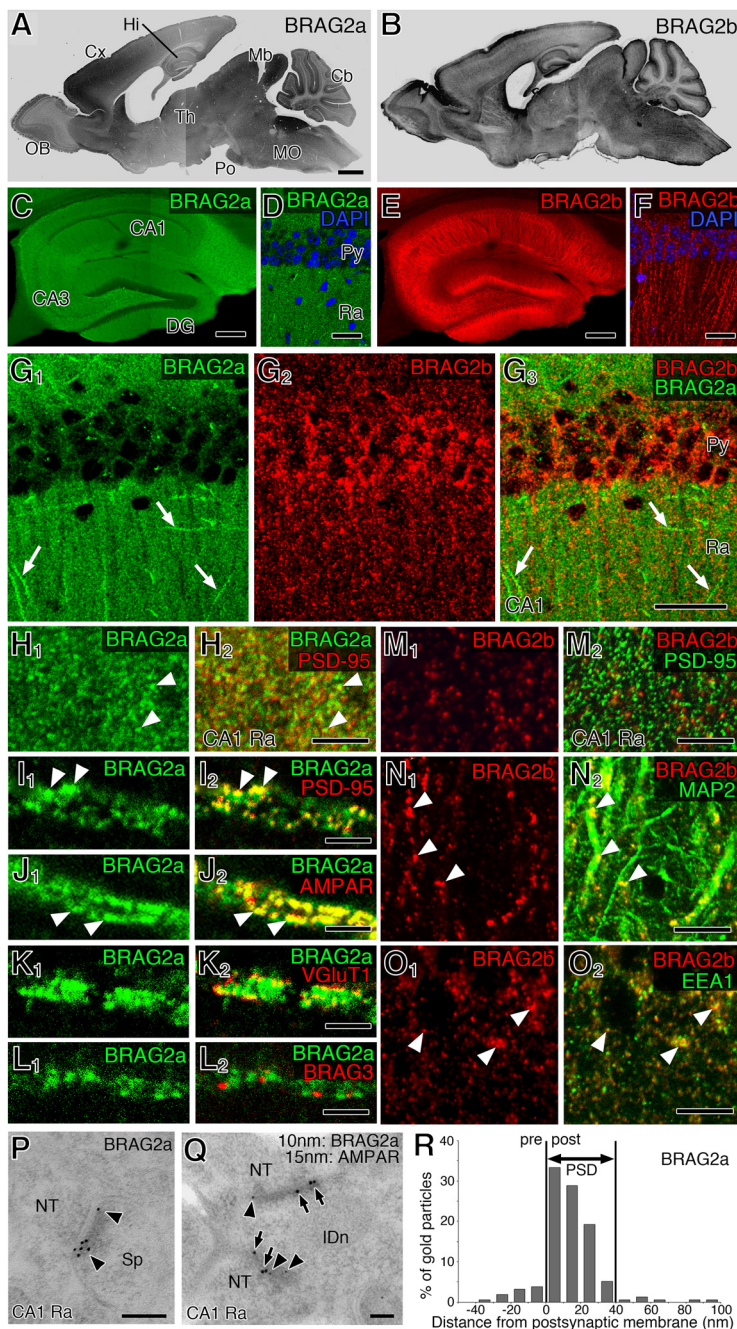


Figure 3. BRAG2a is selectively localized to the excitatory PSD. *A, B*, Immunoperoxidase staining of the adult mouse brain for BRAG2a (*A*) and BRAG2b (*B*) antibodies. *C–G₃*, Immunofluorescence staining of the hippocampal formation for BRAG2a (*C, D, G₁*) and BRAG2b (*E, F, G₂*). Arrows in *G_{1–G₃}* indicate signals for BRAG2a along the dendrites of interneurons. *H_{1–L₂}*, Double immunofluorescence staining for BRAG2a and PSD-95 (*H_{1–I₂}*), AMPAR (*J_{1, J₂}*), VGLUT1 (*K_{1, K₂}*), or BRAG3 (*L_{1, L₂}*) in the neuropil region (*H_{1, H₂}*) and along the dendrites of interneurons (*I_{1–L₂}*). Note that signals for BRAG2a (*H_{1–J₂}*, arrowheads) overlapped with those for PSD-95 and AMPAR, but not with those for VGLUT1 or BRAG3. *M_{1–O₂}*, Double immunofluorescence staining for BRAG2b and PSD-95 (*M_{1, M₂}*), MAP2 (*N_{1, N₂}*), or EEA1 (*O_{1, O₂}*) in the hippocampal CA1 region. Note that signals for BRAG2b (*N_{1–O₂}*, arrowheads) overlapped with those for MAP2 and EEA1 in the pyramidal cell dendrites, but not with those for PSD-95. *P, Q*, Postembedding immunoelectron microscopy of asymmetrical synapses in the hippocampal CA1 region for BRAG2a (*P*), and for BRAG2a and AMPAR (*Q*). Arrowheads (*P, Q*) and arrows (*Q*) point to 10 and 15 nm gold particles for BRAG2a and AMPAR, respectively. *R*, Perpendicular distribution of gold particles for BRAG2a from the postsynaptic membrane. The outer leaflet of the postsynaptic membrane is defined as 0 nm with plus and minus values in the postsynaptic and presynaptic sides, respectively. Note the selective accumulation of BRAG2a signals in the PSD. CA1 and CA3, CA1 and CA3 regions of Ammon's horn; Cb, cerebellum; Cx, cerebral cortex; DG, dentate gyrus; Hi, hippocampus; IDn, dendrite of interneuron; NT, nerve terminal; OB, olfactory bulb; Mb, midbrain; MO, medulla oblongata; Po, pontine nuclei; Py, pyramidal cell layer; Ra, stratum radiatum; Sp, stratum radiatum; Th, thalamus. Scale bars: *A, 1* mm; *C, E, 200* μ m; *D, F, G, 50* μ m; *H, M, N, O, 20* μ m; *I–L, 2* μ m; *P, Q, 100* nm.

To examine the subcellular localization of BRAG2 isoforms, we produced novel isoform-specific antibodies against their unique C-terminal regions as antigens (Fig. 1A). Immunoblotting of mouse brain lysates using an anti-BRAG2a antibody detected two immunoreactive bands of 160 and 140 kDa, and anti-BRAG2b detected a single band of 110 kDa (Fig. 2A). All of these three bands were detected by the anti-panBRAG2 antibody raised between a common central region containing the IQ and Sec7 domains (Sakagami et al., 2013; Figs. 1A, 2A). The specificity of the antibodies was further verified by immunoblotting and immunofluorescence analyses using HeLa cells expressing FLAG-BRAG2a or FLAG-BRAG2b exogenously (Fig. 2B–H). Although immunoperoxidase staining of the mouse brain using isoform-specific antibodies produced a widespread labeling pattern consistent with their gene expression patterns (Fig. 3A,B), immunofluorescence revealed distinct subcellular labeling of the two isoforms in the hippocampal formation at a higher magnification (Fig. 3C–G). In the hippocampal CA1 region, the two isoform-specific antibodies yielded minimally overlapping immunoreactive puncta in the cell bodies and neuropils of pyramidal cells (Fig. 3G). BRAG2a-immunoreactive puncta overlapped well with PSD-95 (Fig. 3H,I) and AMPARs (Fig. 3J), which are excitatory postsynaptic markers, in close apposition to vesicular glutamate transporter 1 (VGLUT1), a glutamatergic presynaptic marker (Fig. 3K). However, they did not overlap with BRAG3/Iqsec3, another BRAG/Iqsec member that localizes specifically to inhibitory postsynapses (Fukaya et al., 2011; Fig. 3L). Conversely, BRAG2b-immunoreactive puncta were distributed intracellularly in cell bodies and dendritic processes labeled with MAP2 (Fig. 3N), a neuron-specific cytoskeletal protein enriched in cell bodies and dendrites, and largely colocalized with EEA1, a marker of a subpopulation of early sorting endosomes (Fig. 3O). However, they did not overlap with BRAG2a or PSD-95 (Fig. 3G,M). These findings suggest that BRAG2a and BRAG2b are differentially localized to excitatory synapses and intracellular membrane structures, respectively.

To further examine the synaptic localization of BRAG2a at the ultrastructural level, we performed postembedding immunoelectron microscopy of the hippocampal CA1 region. Immunogold-labeled BRAG2a was exclusively detected at the PSD of asymmetrical synapses, which were simultaneously labeled by an anti-AMPA antibody, in the CA1 stratum radiatum (Fig. 3P,Q). Inside the PSD of asymmetric synapses, two-thirds of the Immunogold-labeled BRAG2a were perpendicularly distributed in 0–20 nm bins postsynaptic from the outer leaflet of the postsynaptic plasma membrane (Fig. 3R).

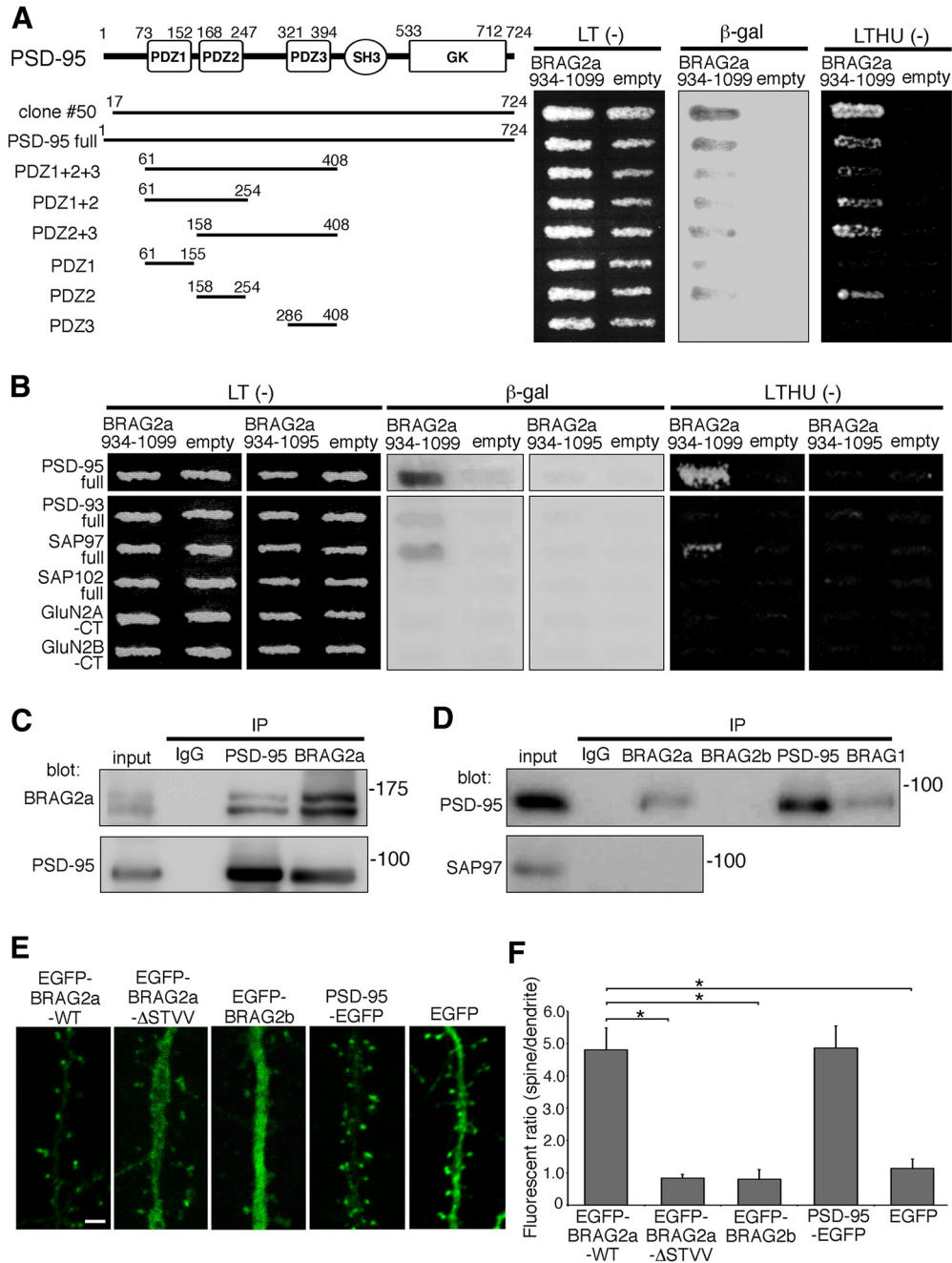


Figure 4. The interaction of BRAG2a with PSD-95 is required for its synaptic targeting. **A**, Schematic representation of the domain structure of PSD-95 and its fragments used in the yeast two-hybrid assays. The yeast strain MaV203 was transformed with the BRAG2a-specific C-terminal region (934–1099) and the indicated combinations of PSD-95 constructs, and then plated on synthetic complete medium lacking leucine and tryptophan [LT(–)] or leucine, tryptophan, histidine and uracil [LTHU(–)]. Interactions were assessed by β -galactosidase activity (β -gal) and the ability to grow on LTHU(–) medium. Note the interaction of BRAG2a with the PSD-95 fragments containing PDZ2. **B**, Interaction of the C-terminal PDZ-binding motif of BRAG2a with PSD-95 and other PSD proteins. Note the disruption of the interaction after deletion of the last four C-terminal amino acids (STVV) containing the PDZ-binding motif of BRAG2a (BRAG2a 934–1095). The C-terminal PDZ-binding motif of BRAG2a also interacted with SAP97, but not PSD-93, SAP102, GluN2A, or GluN2B. **C**, **D**, Immunoprecipitation (IP) assays. Triton X-100-soluble hippocampal P2 fractions were subjected to immunoprecipitation with anti-PSD-95, anti-BRAG2a, anti-BRAG2b, anti-BRAG1, or normal rabbit IgG and immunoblotting with anti-BRAG2a (**C**), anti-PSD-95 (**C**, **D**), or anti-SAP97 (**D**) antibodies. Note the coimmunoprecipitation of PSD-95 with BRAG2a and BRAG1, but not with BRAG2b from hippocampal lysates. **E**, **F**, Synaptic targeting assays of EGFP-tagged BRAG2a-WT, BRAG2a- Δ STVV, BRAG2b, PSD-95, and EGFP alone in cultured hippocampal neurons at DIV15 (**E**); and quantification of the ratio of EGFP fluorescence signals in spine heads versus dendritic shafts (**F**). Note that EGFP-BRAG2a- Δ STVV, EGFP-BRAG2b, and EGFP alone showed the uniform distribution throughout spiny dendrites in contrast to the preferential synaptic localization of EGFP-BRAG2a-WT and PSD-95-EGFP. The spine/dendrite ratios of the EGFP fluorescent intensity were obtained from 100 measurements from five transfected neurons. These results were confirmed by two independent experiments. * $p < 0.001$ (t test). Scale bar, 2 μ m.

These results indicate that BRAG2a is a core PSD protein at hippocampal excitatory synapses, consistent with previous proteomic analyses of the PSD (Jordan et al., 2004; Peng et al., 2004) and immunoblotting of mouse brain fractions (Scholz et al., 2010).

BRAG2a is targeted to postsynapses through its direct interaction with PSD-95

To obtain mechanistic insight into specific localization and functions of BRAG2a at postsynapses, we performed yeast two-hybrid screening of a mouse brain cDNA library using BRAG2a-

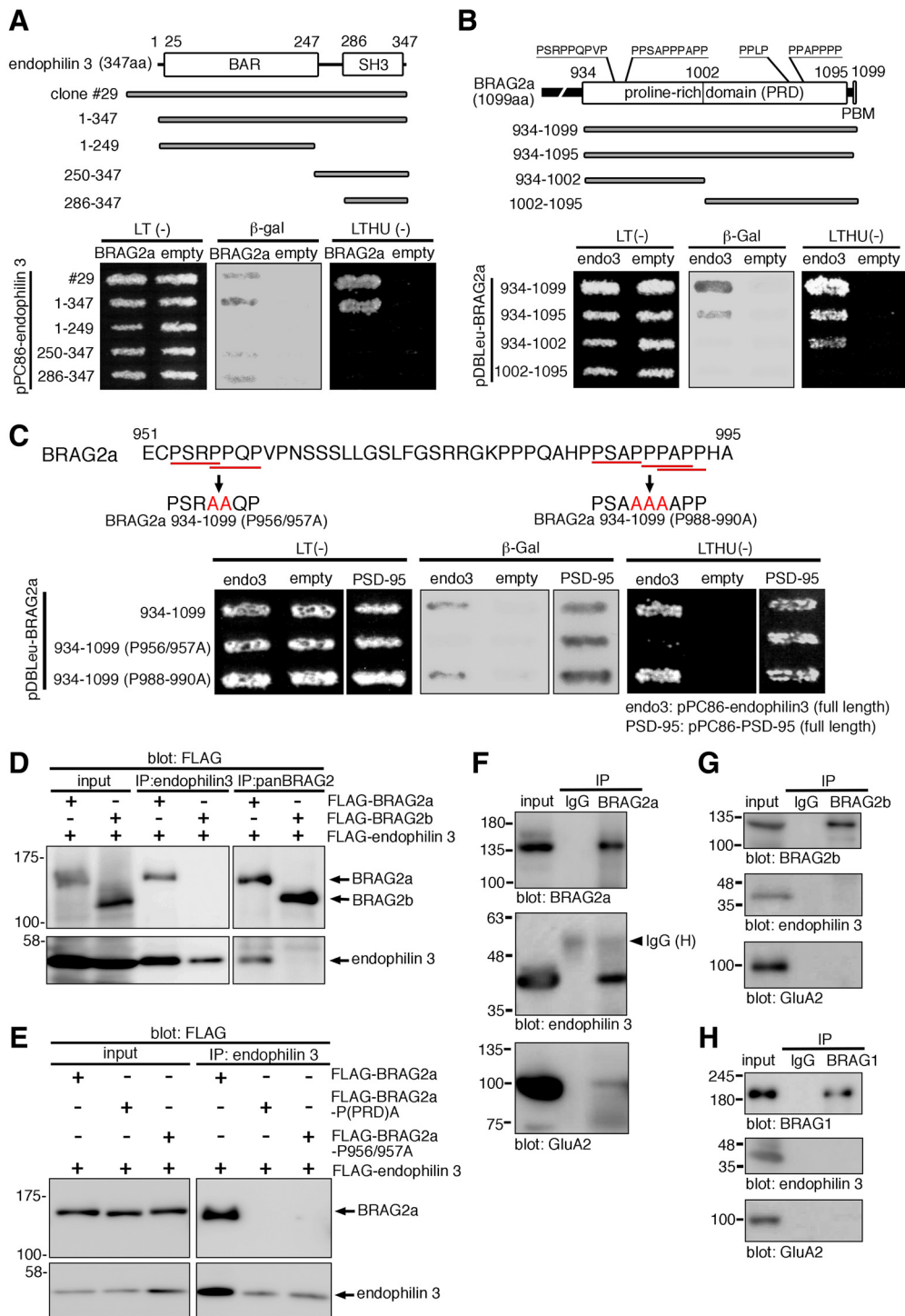


Figure 5. BRAG2a directly interacts with endophilin 3. **A, B**, Schematic representation of the domain structure of endophilin 3 (**A**), BRAG2a (**B**), and their fragments used in the yeast two-hybrid assays. Note the interaction between the PRD (934–1002) of BRAG2a and the SH3 domain of endophilin 3. **C**, Amino acid sequence of the BRAG2a PRD (951–995) and positions of substitution mutations used in the yeast two-hybrid assays. Red bars indicate the putative consensus sequence (PxxP) for SH3 domain binding in the PRD. The P956/957A mutation of BRAG2a disrupted the interaction with endophilin 3. **D**, Immunoprecipitation assays. HeLa cells expressing FLAG-endophilin 3 and FLAG-BRAG2a or FLAG-BRAG2b were immunoprecipitated with antibodies against BRAG2 or endophilin 3, and were subjected to immunoblotting with an anti-FLAG antibody. **E**, Immunoprecipitation assays. HeLa cells expressing FLAG-endophilin3 and FLAG-BRAG2a, FLAG-BRAG2a-P(PRDA), or FLAG-BRAG2a-P956/957A were immunoprecipitated with the anti-endophilin 3 antibody and subjected to immunoblotting with the anti-FLAG antibody. **F–H**, Immunoprecipitation of mouse hippocampal lysates. Triton X-100-soluble mouse hippocampal P2 fractions were immunoprecipitated with anti-BRAG2a (**F**), anti-BRAG2b (**G**), anti-BRAG1 (**H**), or normal rabbit IgG, and were subjected to immunoblotting with anti-BRAG2a, anti-BRAG2b, anti-BRAG1, anti-endophilin 3, and anti-GluA2 antibodies. Note the immunoprecipitable complex formation of BRAG2a, but not BRAG2b or BRAG1, with endophilin 3 and GluA2 in the mouse hippocampus.

specific C-terminal 166 aa (BRAG2a 934–1099) as bait (Fig. 1A), and isolated a cDNA clone encoding PSD-95 (Fig. 4A). Further yeast two-hybrid assays revealed the second PDZ domain of PSD-95 (PDZ2) is the minimal region that interacts with

BRAG2a (Fig. 4A). As expected by the presence of a type I PDZ-binding motif (STVV) at the C-terminus of BRAG2a, deletion of its last four C-terminal amino acids [BRAG2a (934–1095)] abolished the β -galactosidase activity and prototrophy for histidine

and uracil, confirming that the PDZ-binding motif of BRAG2a is required for its interaction with PSD-95 (Fig. 4B). Further yeast two-hybrid assays revealed that BRAG2a (934–1099) interacted with SAP97 but not PSD-93 or SAP102 (Fig. 4B). Although BRAG2 reportedly interacts with NMDARs, particularly GluN2A (Elagabani et al., 2016), coexpression of BRAG2a (934–1099) and the C-terminal cytoplasmic regions of GluN2A or GluN2B in yeasts did not yield positive interactions (Fig. 4B), suggesting that the C-terminal BRAG2a region used as bait does not mediate the interaction of BRAG2 with NMDARs. In immunoprecipitation assays, PSD-95 was efficiently coimmunoprecipitated with BRAG2a, but not with BRAG2b, from the Triton X-100-soluble P2 fraction of the mouse brain, and vice versa (Fig. 4C,D). By contrast, anti-BRAG2a IgG did not immunoprecipitate a detectable level of SAP97 under the same condition (Fig. 4D). In the control experiment, BRAG1 was coimmunoprecipitated with PSD-95 (Fig. 4D), consistent with a previous report (Sakagami et al., 2008). These results indicate the presence of a BRAG2a and PSD-95 protein complex in the brain.

To examine whether the interaction of BRAG2a with PSD-95 is required for its synaptic localization, cultured hippocampal neurons were transfected with EGFP-BRAG2a, EGFP-BRAG2a- Δ STVV, EGFP-BRAG2b, PSD-95-EGFP, or EGFP alone (Fig. 4E). Quantification of the ratio of EGFP fluorescence in spines versus dendritic shafts revealed that EGFP-BRAG2a was accumulated fivefold more in spines than in dendritic shafts to the same extent as PSD-95-EGFP (Fig. 4E,F). By contrast, EGFP-BRAG2a- Δ STVV and EGFP-BRAG2b exhibited homogeneous distribution throughout spines and dendritic shafts, as was the case for EGFP (Fig. 4E,F; mean \pm SD; EGFP-BRAG2a-WT: 4.807 ± 0.679 ; EGFP-BRAG2a- Δ STVV: 0.839 ± 0.109 , $p = 0.0006$, t test; EGFP-BRAG2b: 0.803 ± 0.301 , $p = 0.0007$; PSD-95-EGFP: 4.866 ± 0.671 , $p = 0.919$; EGFP: 1.139 ± 0.286 , $p = 0.001$). These results suggest that BRAG2a is targeted to postsynapses through its direct interaction with PSD-95.

BRAG2a interacts with endophilin 3

In addition to PSD-95, we isolated several independent cDNA clones encoding endophilin 1 (A1) and endophilin 3 (A3) by two-hybrid screening (Fig. 5A). Endophilin is a family of BAR and SH3 domain-containing proteins implicated in clathrin-dependent endocytosis (Ringstad et al., 1997, 1999; Schuske et al., 2003). Because endophilin 1 and 3 are reportedly enriched in presynaptic and postsynaptic compartments, respectively (Chowdhury et al., 2006), we hereafter focused on the interaction between BRAG2a and endophilin 3 at postsynapses.

Yeast two-hybrid assays with BRAG2a and various truncated mutants of endophilin 3 revealed that amino acids 286–347 of

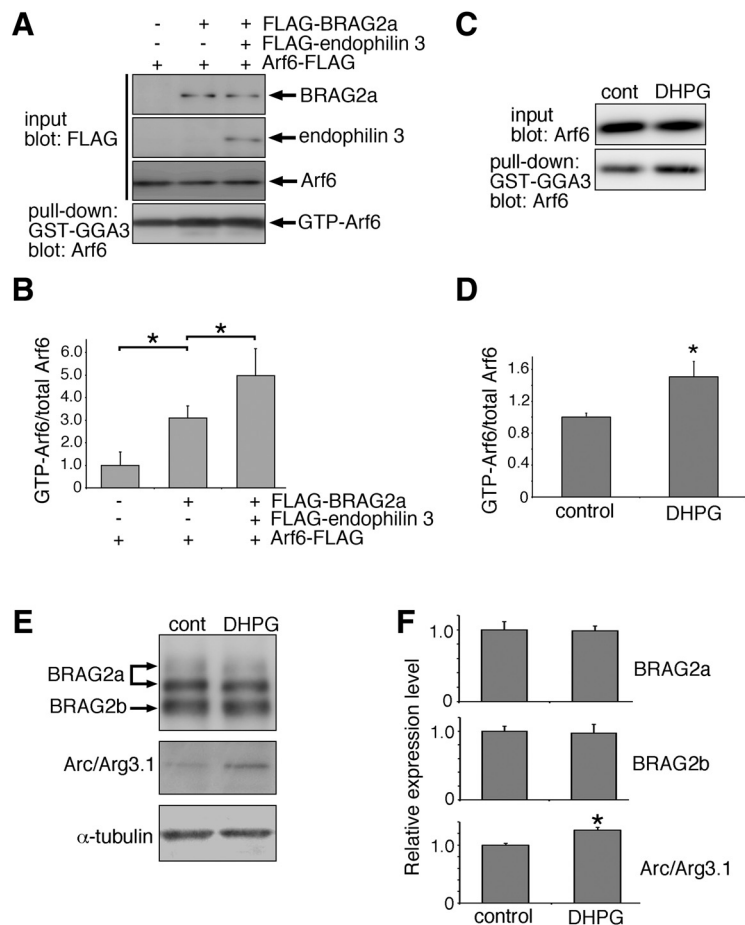


Figure 6. The BRAG2a-endophilin 3 interaction and mGluR stimulation facilitate Arf6 activation. **A, B**, Endophilin 3 enhances BRAG2a-mediated Arf6 activation in HeLa cells. **A**, Representative immunoblotting of Arf6 activation assays using GST-GGA3 from HeLa cells expressing Arf6-FLAG and the indicated combinations of FLAG-BRAG2a and FLAG-endophilin 3. **B**, Quantification of the GTP-Arf6/total Arf6 ratio. Note that coexpression of FLAG-endophilin 3 with FLAG-BRAG2a enhanced BRAG2a-mediated Arf6 activation. **C, D**, DHPG treatment stimulates Arf6 activation in cultured hippocampal neurons at DIV16. **C**, Representative immunoblotting of Arf6 activation assays using GST-GGA3 from cultured hippocampal neurons treated with or without 50 μ M DHPG for 15 min. **D**, Quantification of the GTP-Arf6/total Arf6 ratio. **E, F**, The effect of DHPG treatment on the protein expression of BRAG2a, BRAG2b, and Arc/Arg3.1 in cultured hippocampal neurons at DIV16. **E**, Representative immunoblotting images using anti-panBRAG2, anti-Arc/Arg3.1 and anti- α -tubulin antibodies. **F**, Quantification of the immunoreactive intensity of BRAG2a, BRAG2b, and Arc/Arg3.1. Each immunoreactive intensity was normalized by that of α -tubulin. Note the significant upregulation of Arc/Arg3.1, but not BRAG2a or BRAG2b, in cultured hippocampal neurons treated with DHPG. * $p < 0.05$ (t test). Data for each group were obtained from three culture plates ($n = 3$). These results were confirmed by three (**B, D**) or two (**F**) independent experiments.

endophilin 3 containing the SH3 domain are the minimal region for interacting with BRAG2a, judging from the positive β -galactosidase activity (Fig. 5A). The SH3 domain is known to interact with proline-rich domains (PRDs), particularly those containing the PxxP consensus motif (Alexandropoulos et al., 1995). Of note, the C-terminal region of BRAG2a used as bait contains several PxxP motifs in a proline-rich domain corresponding to amino acids 934–1095 (Fig. 5B). Yeast two-hybrid assays using the full-length endophilin 3 and a truncated C-terminal region of BRAG2a revealed that the former half of the proline-rich domain corresponding to amino acids 934–1002 was responsible for the interaction with endophilin 3 (Fig. 5B). Alanine substitution of proline residues in the PxxP motifs at amino acids 956 and 957 (P956/957A, PSRPPQP \rightarrow PSRAAQP), but not at amino acids 988, 989, and 990 (P988–990A, PSAPPPAPP \rightarrow PSAAAAAPP), abolished the interaction with endophilin 3 (Fig. 5C). These results

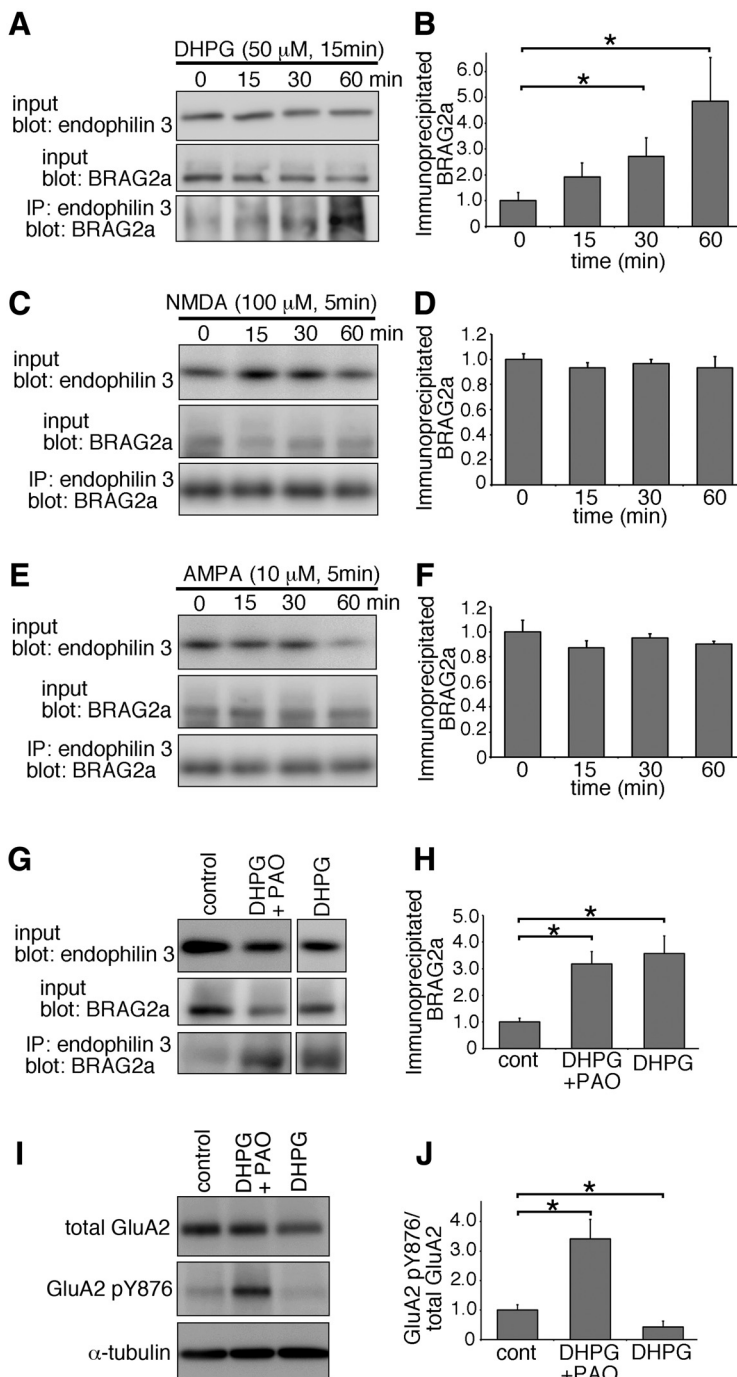


Figure 7. mGluR stimulation facilitates the formation of BRAG2a–endophilin 3 complex. **A–F**, Immunoprecipitation assays. Cultured hippocampal neurons at various time points (0, 15, 30, and 60 min) following the treatment with 50 μ M DHPG for 15 min (**A, B**), 100 μ M NMDA for 5 min (**C, D**), or 10 μ M AMPA for 5 min (**E, F**) at DIV16 were immunoprecipitated with anti-endophilin 3 antibody and subjected to immunoblotting with anti-BRAG2a antibody. **B, D, F**, Quantification of the amount of BRAG2a immunoprecipitated with anti-endophilin 3 antibody (**B, D, F**) showed that the treatment with DHPG (**B**) but not NMDA (**D**) or AMPA (**F**) facilitated the formation of BRAG2a–endophilin 3 complex in a time-dependent manner. **G, H**, The effect of tyrosine phosphatase inhibition on mGluR-dependent complex formation between BRAG2a and endophilin 3. **G**, Cultured hippocampal neurons at 45 min following treatment with 50 μ M DHPG in the presence or absence of 15 μ M PAO for 15 min were immunoprecipitated with anti-endophilin 3 antibody and subjected to immunoblotting with anti-BRAG2a antibody. **H**, Note that the tyrosine phosphatase inhibitor had no significant effect on the DHPG-induced formation of BRAG2a–endophilin 3 complex. **I, J**, The effect of tyrosine phosphatase inhibition on the phosphorylation state of tyrosine 876 of GluA2 following DHPG treatment. **I**, Cultured hippocampal neurons at 45 min following treatment with 50 μ M DHPG in the presence or absence of 15 μ M PAO for 15 min were immunoblotted with antibodies against total GluA2, pY876 GluA2, and α -tubulin. **J**, Note that the treatment with PAO significantly inhibited the DHPG-induced dephosphorylation of tyrosine 876 of GluA2 with further enhancement of its phosphorylation state. The immunoreactive intensities of immunoprecipitated BRAG2a were normalized by those of total BRAG2a in input lysates and compared

suggest that BRAG2a can interact with the SH3 domain of endophilin 3 through its canonical PxxP motifs at amino acids 953–959.

To confirm the interaction between BRAG2a and endophilin 3 in mammalian cells, we performed immunoprecipitation assays using HeLa cells cotransfected with FLAG-endophilin 3 and FLAG-BRAG2a or FLAG-BRAG2b (Fig. 5D). FLAG-BRAG2a, but not FLAG-BRAG2b, was efficiently coimmunoprecipitated with endophilin 3, and vice versa (Fig. 5D). Consistent with the results in the two-hybrid assay, neither FLAG-BRAG2a-P(PRD)A nor FLAG-BRAG2a-P956/957A was coimmunoprecipitated with endophilin 3 from the lysates of transfected HeLa cells (Fig. 5E). Despite comparable expression levels of FLAG-endophilin 3 in the lysates among samples, more FLAG-endophilin 3 was consistently immunoprecipitated by anti-endophilin 3 antibody when HeLa cells were cotransfected with FLAG-endophilin 3 and FLAG-BRAG2a, suggesting that the BRAG2–endophilin 3 interaction may affect the conformation or dimerization status of endophilin 3, thereby affecting the immunoprecipitation efficiency. Finally, immunoprecipitation of the mouse brain revealed that the anti-BRAG2a, but not anti-BRAG2b antibody, immunoprecipitated endogenous endophilin 3 and GluA2 from the Triton X-100-soluble P2 fraction (Fig. 5F,G). In the reciprocal immunoprecipitation, the anti-endophilin 3 antibody failed to immunoprecipitate detectable amounts of BRAG2a (data not shown), suggesting that only a limited fraction of endophilin 3 forms a protein complex with BRAG2a in the brain. By contrast, the anti-BRAG1 antibody failed to immunoprecipitate endophilin 3 or GluA2 under the same experimental condition (Fig. 5H). These results suggest that BRAG2a specifically forms a protein complex with endophilin 3 and AMPARs in the brain.

BRAG2a–endophilin 3 interaction enhances the GEF activity of BRAG2a toward Arf6

To examine the effect of the BRAG2a and endophilin 3 interaction on the GEF activity of BRAG2a, HeLa cells were transfected with Arf6-FLAG, FLAG-BRAG2a, and FLAG-endophilin 3, and subjected to Arf6 pull-down assays using a GST fusion protein of the GGA3-GAT domain, which can specifically bind to GTP-bound Arfs (Nakayama and Takatsu, 2005), and immunoblotting with anti-Arf6 antibody. Co-expression of Arf6 and BRAG2a significantly increased the amount of GTP-Arf6 by threefold

with control. The immunoreactive intensities of pY876 GluA2 was normalized by those of total GluA2, and compared with control. * $p < 0.05$ (t test). Data for each group were obtained from three culture plates ($n = 3$). These results were confirmed by three independent experiments.

compared with Arf6 alone, whereas simultaneous expression of Arf6, BRAG2a, and endophilin 3 further increased the amount of GTP-Arf6 by fivefold compared with Arf6 alone (Fig. 6A,B; mean \pm SD; Arf6 alone: 1.000 ± 0.580 ; Arf6 and BRAG2a: 3.090 ± 0.550 , $p = 0.007$, t test; Arf6, BRAG2a, and endophilin 3: 4.990 ± 1.190 , $p = 0.033$; $n = 3$ plates for each group). Of note, the expression levels of FLAG-BRAG2a in HeLa cells cotransfected with or without endophilin 3 were comparable (Arf6 and BRAG2a: 17.895 ± 4.230 ; Arf6, BRAG2a, and endophilin 3: 16.470 ± 4.506 , $p = 0.710$, t test; $n = 3$ plates for each group), excluding the possibility that FLAG-BRAG2a levels affected GTP-Arf6 levels. These results suggest that the interaction of BRAG2a with endophilin 3 enhances its GEF activity toward Arf6.

mGluR1/5 stimulation triggers the protein complex formation between BRAG2a and endophilin 3

Stimulation of mGluR1/5 reportedly triggers the interaction of BRAG2 with GluA2 and the subsequent activation of Arf6, thereby leading to the internalization of surface AMPARs (Scholz et al., 2010). Consistently, the amount of GTP-Arf6 was significantly increased by 1.5-fold in cultured hippocampal neurons at 45 min following the treatment with $50 \mu\text{M}$ DHPG for 15 min (Fig. 6C,D; mean \pm SD; control: 1.000 ± 0.050 ; DHPG: 1.504 ± 0.194 , $p = 0.011$, t test; $n = 3$ plates for each group). As hippocampal mGluR-dependent LTD is required for rapid protein synthesis in dendrites (Huber et al., 2000), we also examined the effect of mGluR stimulation on the protein expression level of BRAG2 in total lysates of cultured neurons. Although Arc/Arg3.1 was increased by 25.7%, as reported previously (Niere et al., 2012), BRAG2 did not show any significant changes in its protein expression at 60 min after DHPG treatment (Fig. 6E,F; mean \pm SD; BRAG2a/control: 1.000 ± 0.112 ; BRAG2a/DHPG: 0.981 ± 0.070 , $p = 0.785$, t test; BRAG2b/control: 1.000 ± 0.071 ; BRAG2b/DHPG: 0.970 ± 0.130 , $p = 0.698$; Arc/control: 1.000 ± 0.003 ; Arc/DHPG: 1.257 ± 0.049 , $p = 0.001$; $n = 3$ plates for each group), indicating that DHPG-induced Arf6 activation does not correlate with BRAG2 expression level. Under these experimental conditions, the amount of BRAG2a coimmunoprecipitated with endophilin 3 was steadily increased until 60 min following DHPG treatment in a time-dependent manner (Fig. 7A,B; mean \pm SD; 0 min: 1.000 ± 0.310 ; 15 min: 1.906 ± 0.552 , $p = 0.113$, t test; 30 min: 2.712 ± 0.721 , $p = 0.047$; 60 min: 4.837 ± 1.692 , $p = 0.045$; $n = 3$ plates for each group), suggesting that mGluR stimulation triggers the interaction between BRAG2a and endophilin 3 in cultured hippocampal neurons. By contrast, treatment with $100 \mu\text{M}$ NMDA for 5 min or $10 \mu\text{M}$ AMPA for 5 min did not induce the interaction between BRAG2a and endophilin 3 (Fig. 7C–F; mean \pm SD; NMDA: 0 min, 1.000 ± 0.042 ; 15 min, 0.933 ± 0.039 , $p = 0.113$, t test; 30 min, 0.964 ± 0.035 ,

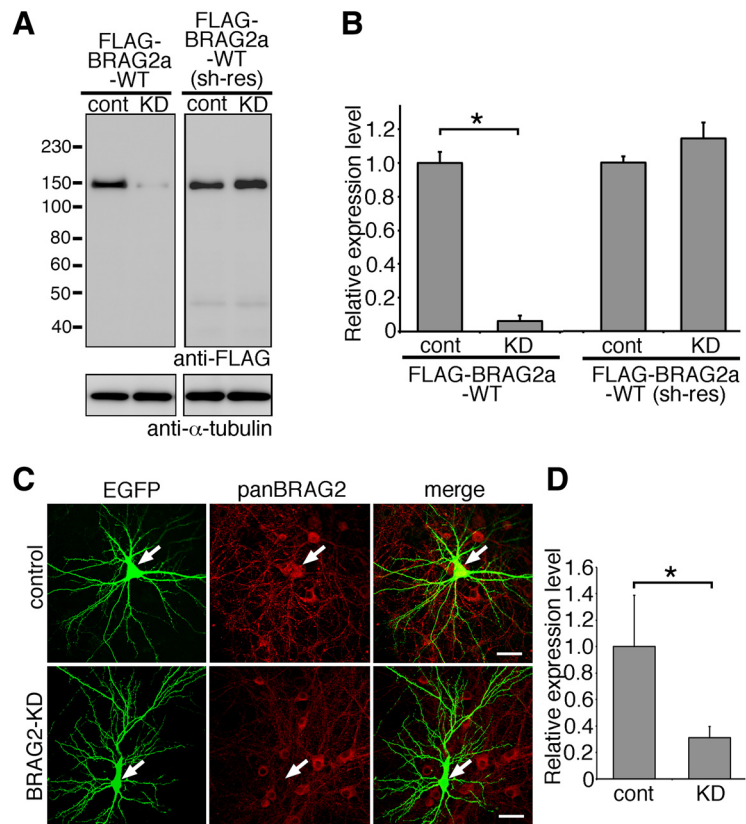


Figure 8. The efficiency of shRNA for BRAG2. **A, B**, Verification of BRAG2 knockdown efficiency by immunoblotting. **A**, HeLa cells were transfected with an shRNA expression vector for BRAG2 (KD) or luciferase [control (cont)] together with FLAG-BRAG2a-WT or shRNA-resistant (sh-res) FLAG-BRAG2a-WT. **B**, Quantification of the BRAG2 knockdown efficiency. The ratio of the immunoreactivity for FLAG-BRAG2a to that for α -tubulin for each group was normalized and compared with control. $*p < 0.05$ (t test). Data for each group were obtained from three culture plates ($n = 3$). These results were confirmed by two independent experiments. **C, D**, Verification of BRAG2 knockdown efficiency by immunofluorescence in cultured hippocampal neurons. Neurons were transfected with BRAG2-KD or control shRNA at DIV13 and subjected to immunofluorescence with anti-EGFP and anti-panBRAG2 antibodies at DIV15. Note the marked attenuation of immunofluorescence for endogenous BRAG2 in BRAG2-KD-transfected but not control-transfected neurons (**C**). Arrows indicate shRNA-transfected neurons visualized by simultaneous expression of EGFP. Scale bars, $20 \mu\text{m}$. Quantification of the BRAG2 knockdown efficiency in transfected neurons (**D**). The immunoreactive intensity of BRAG2 was normalized and compared with control. $*p < 0.05$ (t test). Data for each group were obtained from 20 neurons from three plates. These results were confirmed by three independent experiments.

$p = 0.313$; 60 min, 0.930 ± 0.091 , $p = 0.293$; AMPA: 0 min, 1.000 ± 0.092 ; 15 min, 0.872 ± 0.054 , $p = 0.106$; 30 min, 0.948 ± 0.034 , $p = 0.410$; 60 min, 0.903 ± 0.022 , $p = 0.149$; $n = 3$ plates for each group). DHPG-induced tyrosine dephosphorylation of GluA2 at Y876 relies on the interaction between BRAG2 and GluA2 (Scholz et al., 2010). To examine whether the interaction between BRAG2 and GluA2 could affect DHPG-induced complex formation of BRAG2a with endophilin 3, cultured neurons were stimulated with DHPG in the presence of a tyrosine phosphatase inhibitor, PAO, and subjected to immunoprecipitation (Fig. 7G,H). Although treatment with PAO blocked DHPG-induced tyrosine dephosphorylation of GluA2 at Y876 with further enhancement of its phosphorylation state (Fig. 7I,J; mean \pm SD; control: 1.000 ± 0.173 ; DHPG + PAO: 3.417 ± 0.657 , $p = 0.004$, t test; DHPG: 0.432 ± 0.196 , $p = 0.019$; $n = 3$ plates for each group), it did not affect the DHPG-induced interaction between BRAG2a and endophilin 3 (Fig. 7G,H; mean \pm SD; control: 1.000 ± 0.147 ; DHPG + PAO: 3.175 ± 0.467 , $p = 0.002$, t test; DHPG: 3.568 ± 0.656 , $p = 0.003$; $n = 3$ plates for each group), suggesting that the BRAG2a–endophilin 3 interaction takes place independently of the tyrosine dephosphorylation of GluA2.

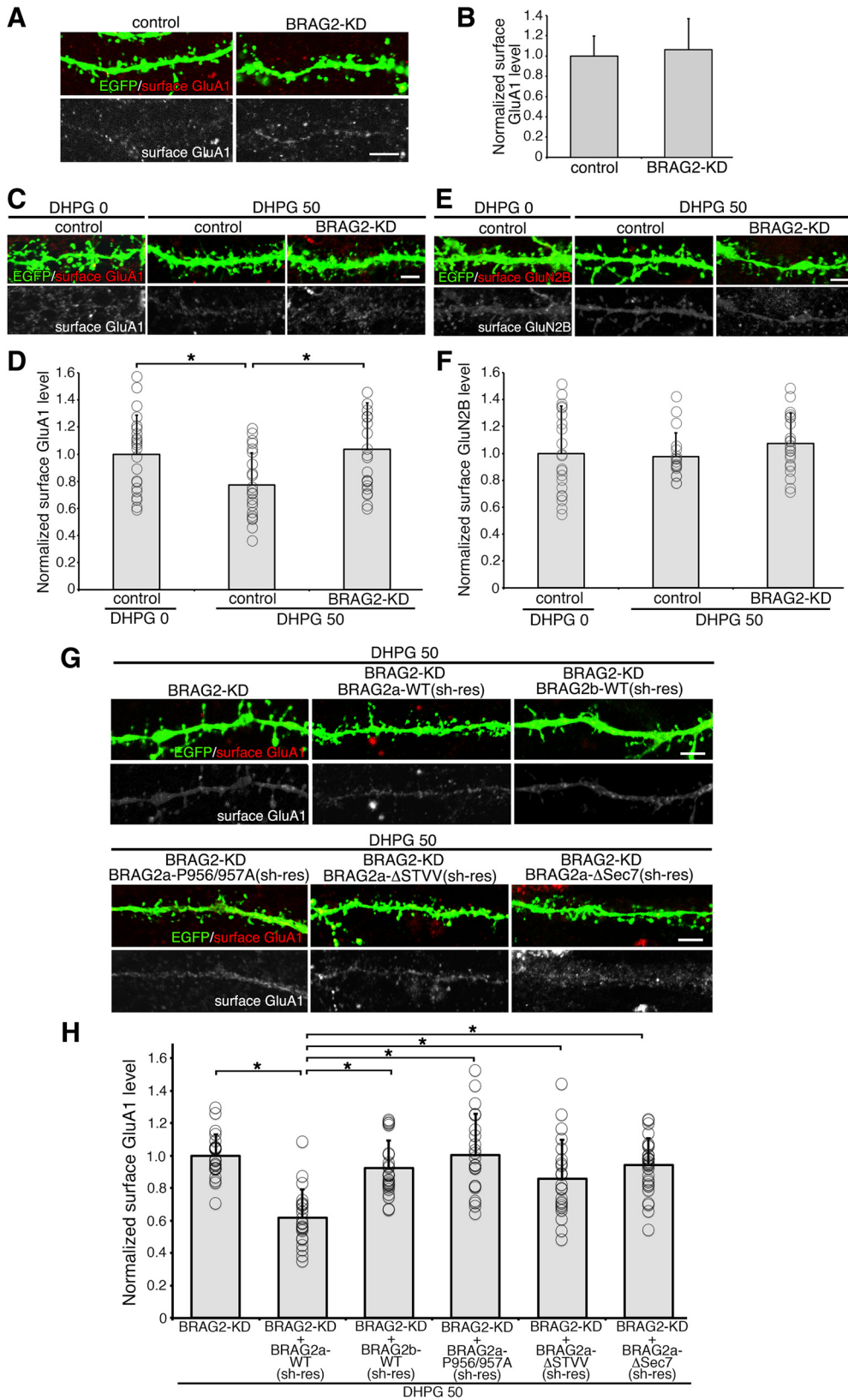


Figure 9. The interaction of BRAG2a with endophilin 3 and PSD-95 is important for the mGluR-dependent decrease in AMPAR surface level. **A, B**, The effect of BRAG2 knockdown on basal surface GluA1 level. **A**, Representative immunofluorescence images of dendritic shafts and spines of cultured hippocampal neurons transfected with shBRAG2 (BRAG2-KD) or shControl (control) vectors at DIV14 and subjected to surface AMPAR labeling with anti-GluA1 (extracellular) antibody at DIV16. **B**, Quantification of surface GluA1 levels. Immunofluorescence intensity of surface GluA1 in BRAG2-KD-transfected neurons was normalized to that in the control-transfected neurons. Note that knockdown of BRAG2 did not affect the basal surface GluA1 levels. **C, D**, The effect of BRAG2 knockdown on surface GluA1 levels following DHPG treatment. **D**, Quantification of surface GluA1 levels. Note that BRAG2 knockdown blocked the decrease in surface GluA1 levels following 50 μ M DHPG treatment (DHPG 50). Asterisks indicate statistical significance (one-way ANOVA; $F_{(2,61)} = 4.507$, $p = 0.0149$; followed by Tukey–Kramer *post hoc* test, $*p < 0.05$). **E, F**, The effect of BRAG2 knockdown on surface GluA2B levels following DHPG treatment. **E**, Representative immunofluorescence images of dendritic shafts and spines of BRAG2-KD or control

BRAG2a–endophilin 3 interaction is required for mGluR-stimulated internalization of AMPARs

Endophilin 3 is implicated in the endocytosis of AMPARs in the hippocampus through ternary interaction with dynamin and Arc/Arg3.1 (Chowdhury et al., 2006) or oligophrenin-1 (Nadif Kasri et al., 2011). To examine the functional role of the interaction between BRAG2a and endophilin 3 in the mGluR-dependent internalization of AMPARs, we prepared an shRNA vector for BRAG2 (shBRAG2), which targets both BRAG2 isoforms and simultaneously expresses EGFP to visualize transfected cells under an independent promoter. HeLa cells were transfected with shBRAG2 or shRNA for luciferase (shControl), together with FLAG-BRAG2a-WT or shRNA-resistant (sh-res) FLAG-BRAG2a-WT. Expression of shBRAG2 effectively downregulated FLAG-BRAG2a-WT, compared with that of the control shRNA, without affecting the expression of shRNA-resistant BRAG2a-WT (Fig. 8A,B; mean \pm SD; FLAG-BRAG2a-WT, control: 1.000 ± 0.063 ; BRAG2-KD, 0.061 ± 0.035 , $p < 0.0001$, t test; FLAG-BRAG2a-WT (sh-res), control, 1.000 ± 0.037 ; BRAG2-KD, 1.142 ± 0.093 , $p = 0.070$; $n = 3$ plates for each group). Furthermore, the expression of shBRAG2 markedly reduced immunolabeling of endogenous BRAG2 in transfected neurons compared with the neighboring untransfected neurons on the same culture dish or neurons transfected with shControl (Fig. 8C,D; mean \pm SD; control, 1.000 ± 0.387 , $n = 20$ neurons; BRAG2-KD, 0.312 ± 0.083 , $n = 20$, $p < 0.0001$, t test).

After establishing the shRNA specificity, cultured hippocampal neurons transfected with shBRAG2 or shControl were stimulated with DHPG to chemically induce mGluR-dependent LTD, and then were subjected to labeling of surface AMPARs and NMDARs using antibodies against the extracellular N-terminus of GluA1 and GluN2B subunits, respectively. Before stimulation, there were no apparent differences in basal surface GluA1 levels between shBRAG2-transfected and shControl-transfected neurons (Fig. 9A,B; mean \pm SD; control, 1.000 ± 0.197 , $n = 20$ neurons; BRAG2-KD, 1.062 ± 0.305 , $p > 0.05$, t test; $n = 20$). DHPG stimulation resulted in $\sim 20\%$ decrease in surface GluA1 levels in shControl-transfected neurons, whereas BRAG2 knockdown completely suppressed this effect (Fig. 9C,D; one-way ANOVA, $F_{(2,61)} = 4.507$, $p = 0.0149$; followed by Tukey–Kramer *post hoc* test; mean \pm SD; DHPG 0/control: 1.000 ± 0.287 , $n = 22$ neurons; DHPG 50/control: 0.782 ± 0.246 , $n = 20$; DHPG 50/BRAG2 KD: 1.038 ± 0.342 , $n = 22$), consistent with a previous

report (Scholz et al., 2010). By contrast, surface GluN2B levels were not affected by DHPG treatment or BRAG2 knockdown (Fig. 9E,F; one-way ANOVA, $F_{(2,59)} = 0.964$, $p = 0.387$; mean \pm SD; DHPG 0/control: 1.000 ± 0.311 , $n = 20$ neurons; DHPG 50/control: 0.972 ± 0.166 , $n = 20$; DHPG 50/BRAG2 KD: 1.070 ± 0.209 , $n = 22$). The BRAG2 knockdown effect on surface GluA1 levels was completely abolished by cotransfection of BRAG2a-WT with shBRAG2, suggesting the specific effect of the shRNA (Fig. 9G,H). Furthermore, cotransfection of BRAG2b-WT, BRAG2a-P956/957A, BRAG2a- Δ STVV, or BRAG2a- Δ Sec7 with shBRAG2 did not rescue the phenotype caused by BRAG2 knockdown (Fig. 9G,H; one-way ANOVA, $F_{(5,138)} = 12.822$, $p < 0.0001$, followed by Tukey–Kramer *post hoc* test; mean \pm SD; DHPG 50/BRAG2 KD/BRAG2a-WT: 0.617 ± 0.173 , $n = 22$; DHPG 50/BRAG2 KD/BRAG2b: 0.922 ± 0.169 , $n = 25$; DHPG 50/shBRAG2/BRAG2a-P956/957A: 1.004 ± 0.252 , $n = 22$; DHPG 50/shBRAG2/BRAG2a- Δ STVV: 0.857 ± 0.241 , $n = 22$; DHPG 50/shBRAG2/BRAG2a- Δ Sec7: 0.940 ± 0.167 , $n = 28$). Of note, in contrast to BRAG2a- Δ STVV (Fig. 4E), BRAG2a-P956/957A, and BRAG2a- Δ Sec7 mutants retained the ability of synaptic targeting in transfected cultured neurons (Fig. 10A–D; mean \pm SD; EGFP-BRAG2a-P956/957A: 4.282 ± 2.213 ; mCherry: 0.992 ± 0.121 , $p = 0.0002$, t test; EGFP-BRAG2a- Δ Sec7: 7.979 ± 3.079 ; mCherry: 0.893 ± 0.190 , $p < 0.0001$, t test; $n = 3$ plates for each group). Furthermore, BRAG2a- Δ Sec7 mutant was confirmed to lack the ability to interact with GluA2 (Fig. 10E) and to activate Arf6 (Fig. 10F,G; mean \pm SD; Arf6-FLAG/FLAG-BRAG2a-WT: 1.502 ± 0.065 ; Arf6-FLAG/FLAG-BRAG2a- Δ Sec7: 0.367 ± 0.124 , $p = 0.0002$, t test; $n = 3$ plates for each group). These results suggest that BRAG2a plays an isoform-specific role in mGluR-dependent AMPAR internalization through the interaction with endophilin 3 and PSD-95.

Lateral distribution of BRAG2a, endophilin 3, and Arf6 along the postsynaptic membrane from the PSD in dendritic spines

In dendritic spines, endocytic machineries such as AP-2, clathrin, and dynamin are laterally organized along the postsynaptic membrane from the PSD to the endocytic zones (Blanpied et al., 2002; Rácz et al., 2004). To provide an anatomical clue to understand the mechanism by which BRAG2-mediated Arf6 activation leads to clathrin-dependent endocytosis of AMPARs on the postsynaptic membrane, we examined the lateral distribution of BRAG2a, endophilin 3, and Arf6 in comparison with that of PSD-95, GluA1/2, α -adaplin of the AP-2 complex, and clathrin along the postsynaptic plasma membrane by postembedding immunoelectron microscopy, a reliable and sensitive method for quantitatively detecting synaptic proteins (Fukaya et al., 2006; Fig. 11). Immunogold-labeled BRAG2a and PSD-95 were preferentially accumulated at the PSD (Fig. 11A–F). Immunogold-labeled GluA1/2 was also highly concentrated within the PSD (Fig. 11G–I), though a small but discrete number of particles was evenly distributed along the plasma membrane outside the PSD, presumably corresponding to extrasynaptic AMPARs. By contrast, immunogold-labeled Arf6, endophilin 3, and AP-2 (α -adaplin) were widely distributed along the plasma membrane in the PSD and extrasynaptic region, with a higher labeling density along the postsynaptic membrane near the PSD edge (Fig. 11J–R). Conversely, immunogold-labeled clathrin was distributed more densely on the membrane in the extrasynaptic region than in the PSD, with two peaks of immunolabeling at 25–50 and 200–225 nm from the PSD edge (Fig. 11S–U).

←

hippocampal neurons treated with $50 \mu\text{M}$ DHPG and subjected to surface NMDAR labeling with anti-GluN2B (extracellular) antibody. **F**, Quantification of surface GluN2B levels; the immunofluorescence intensities of surface GluN2B in BRAG2-KD and control neurons treated with DHPG were normalized to that in control and DHPG-untreated (DHPG 0) neurons. Note that DHPG treatment did not change surface GluN2B levels in BRAG2-KD or control neurons (one-way ANOVA: $F_{(2,59)} = 0.964$, $p = 0.387$). Data for each surface GluN2B were obtained from 20–22 transfected neurons from three plates, and these results were confirmed by three independent experiments. **G, H**, The effect of coexpression of shBRAG2 and BRAG2a or its mutants on the DHPG-induced decrease in surface GluA1 levels. **G**, Representative immunofluorescence images of dendritic shafts and spines of neurons transfected with BRAG2-KD alone or with BRAG2-KD and sh-res BRAG2a-WT, BRAG2b-WT, BRAG2a-P956/957A, BRAG2a- Δ STVV, or BRAG2a- Δ Sec7. **H**, Quantification of surface GluA1 levels. Note that the BRAG2-knock-down phenotype on DHPG-induced surface GluA1 levels could be rescued by coexpression of shRNA-resistant BRAG2a-WT, but not BRAG2b-WT, BRAG2a-P956/957A, BRAG2a- Δ STVV, or BRAG2a- Δ Sec7. Asterisks indicate statistical significance (one-way ANOVA: $F_{(5,138)} = 12.822$, $p < 0.0001$; followed by Tukey–Kramer *post hoc* test, $*p < 0.05$). Each surface GluA1 data were obtained from three independent experiments, and 20–28 transfected neurons from three plates were analyzed in each experiment. Scale bars, $2 \mu\text{m}$.

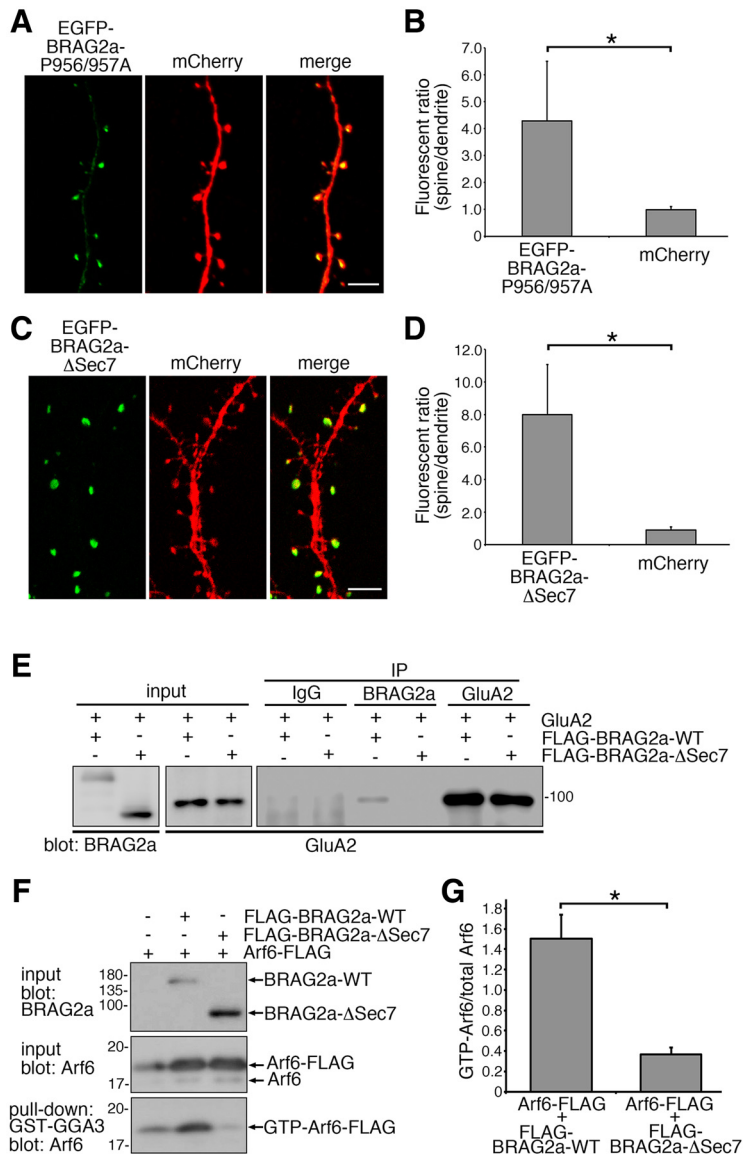


Figure 10. Characterization of BRAG2a-P956/957A and BRAG2a-ΔSec7 mutants. **A–D**, Synaptic targeting assays with the EGFP-tagged BRAG2a-P956/957A and BRAG2a-ΔSec7 mutants in cultured hippocampal neurons at DIV15. Representative immunofluorescence images of the dendritic shaft and spines of neurons transfected with EGFP-BRAG2a-P956/957A (**A**) and EGFP-BRAG2a-ΔSec7 (**C**). The morphology of dendrites and spines was visualized by coexpression of mCherry. Quantification of the ratio of EGFP fluorescence in spines versus dendritic shafts of EGFP-BRAG2a-P956/957A (**B**) and EGFP-BRAG2a-ΔSec7 (**D**). Note that both EGFP-BRAG2a-P956/957A and EGFP-BRAG2a-ΔSec7 were selectively targeted to synapses compared with mCherry. Quantification data for each group were obtained from 100 measurements from five transfected neurons. These results were confirmed by two independent experiments. **E**, Immunoprecipitation assays. HeLa cells expressing GluA2 and FLAG-BRAG2a-WT or FLAG-BRAG2a-ΔSec7 were immunoprecipitated with anti-BRAG2a, anti-GluA2 or normal rabbit IgG, and subjected to immunoblotting with anti-BRAG2a and anti-GluA2 antibodies. Note that BRAG2a-ΔSec7 failed to interact with GluA2. **F, G**, Arf6 activation assays. **F**, Representative immunoblots of Arf6 activation assays using GST-GGA3 from HeLa cells expressing Arf6-FLAG and FLAG-BRAG2a-WT or FLAG-BRAG2a-ΔSec7 mutant. **G**, Quantification of the normalized GTP-Arf6/total Arf6 ratio (**G**). Note that BRAG2a-ΔSec7 lacked the ability to activate Arf6. Data for each group were obtained from three culture plates ($n = 3$). These results were confirmed by three independent experiments. * $p < 0.001$ (t test). Scale bars, $2 \mu\text{m}$.

The effect of mGluR stimulation on the distribution of BRAG2a at the postsynaptic membrane

To examine whether mGluR stimulation could affect the ultrastructural distribution of BRAG2a at the postsynaptic membrane, we performed postembedding immunoelectron microscopy using acute hippocampal slice cultures (Fig. 12). DHPG treatment significantly induced p38 MAPK phosphorylation and

Arc/Arg3.1 upregulation (Fig. 12A,B; mean \pm SD; GluA1/2, control, 1.000 ± 0.128 ; DHPG, 0.938 ± 0.189 , $p = 0.608$, t test; Arc/Arg3.1, control, 1.000 ± 0.207 ; DHPG, 1.417 ± 0.344 , $p = 0.047$; phospho-p38/total p38, control, 1.000 ± 0.245 ; DHPG, 1.897 ± 0.298 , $p = 0.026$, $n = 3$ plates for each group). These results were consistent with previous reports that DHPG induced LTD in the acute hippocampal slice cultures (Bolshakov et al., 2000; Waung et al., 2008). Furthermore, immunogold particles for GluA1/2 in the PSD of asymmetrical axospinous synapses were significantly reduced following DHPG treatment (Fig. 12O–R,U). On the other hand, DHPG treatment did not affect the number of immunogold particles for BRAG2a and PSD-95 in the PSD (Fig. 12C–N,U; mean \pm SD; gold particles/PSD, BRAG2a, control, 1.542 ± 0.309 ; DHPG, 1.599 ± 0.290 , $p = 0.719$, t test; PSD-95, control, 4.857 ± 0.327 ; DHPG, 4.207 ± 0.469 , $p = 0.210$; GluA1/2, control, 2.594 ± 1.747 ; DHPG, 1.748 ± 0.099 , $p = 0.0021$, $n = 3$ slices for each group) or the proportion of extrasynaptic immunogold particles for these proteins (Fig. 12V; percentage of extrasynaptic particles, mean \pm SD; BRAG2a, control, 6.235 ± 1.465 ; DHPG, 5.142 ± 1.374 , $p = 0.399$, t test; PSD-95, control, 3.701 ± 1.073 ; DHPG, 3.218 ± 0.357 , $p = 0.500$; GluA1/2, control, 22.848 ± 5.055 ; DHPG, 21.376 ± 2.231 , $p = 0.668$, $n = 3$ slices for each group). Collectively, these results suggest that BRAG2a forms a protein complex with GluA1/2 and endophilin 3 in the PSD, and does not redistribute to the extrasynaptic region or is only transiently in the extrasynaptic region in response to mGluR stimulation.

Discussion

The present study identified BRAG2 isoform-specific mechanisms of mGluR-dependent AMPAR internalization in hippocampal neurons. Scholz et al. (2010) have previously shown that concomitant ligand binding to AMPAR and dephosphorylation of GluA2 at Tyr876 trigger the interaction between GluA2 and BRAG2, leading to Arf6 activation and subsequent AMPAR internalization during hippocampal mGluR-dependent LTD. Here, we demonstrated that BRAG2a, an alternative isoform with a long C-terminal region containing PRD and a type I PDZ-binding motif, selectively localized to the excitatory PSD of hippocampal neurons through its direct interaction with PSD-95. BRAG2a also interacted with endophilin 3, thereby enhancing its GEF activity toward Arf6. The formation of the BRAG2a–endophilin 3 complex was facilitated by mGluR1/5 activation in cultured hippocampal neurons. The immunoelectron microscopy also

revealed that BRAG2a and PSD-95 were localized exclusively to the PSD without redistribution to the extrasynaptic region in response to mGluR stimulation, whereas Arf6 and endophilin 3 were present in both the PSD and extrasynaptic region in hippocampal neurons. Furthermore, knockdown of BRAG2 blocked the mGluR1/5-stimulated decrease in surface AMPAR levels, which was rescued by introducing wild-type BRAG2a, but not wild-type BRAG2b or BRAG2a mutants lacking the ability to activate Arf6 and to interact with GluA2 (BRAG2a- Δ Sec7) or to interact with endophilin (BRAG2a-P956/957A) or PSD-95 (BRAG2a- Δ STVV), in cultured hippocampal neurons. Together, we propose the following modified model of the BRAG2–Arf6 pathway in mGluR-dependent AMPAR endocytosis: (1) under basal conditions, BRAG2a is localized selectively to the PSD with PSD-95; (2) mGluR1/5 activation triggers the formation of a ternary complex between BRAG2a, AMPARs, and endophilin 3 in the PSD, thereby activating Arf6 on the postsynaptic membrane; (3) GTP–Arf6 recruits clathrin and the AP-2 adaptor complex to promote the assembly and maturation of coated pits through the activation of the lipid modifying enzymes, phosphatidylinositol-4-phosphate 5-kinase (PIP5K) and phospholipase D (PLD), and the direct interaction with AP-2; and (4) after dissociation from BRAG2a, endophilin 3 is released from the PSD, and recruits dynamin and facilitates vesicle budding and membrane scission of coated vesicles containing AMPARs at the endocytic zone. In this model, BRAG2a functions as a platform linking AMPARs to the endocytic molecular machinery through its direct interactions with GluA2 and endophilin 3, thereby ensuring the specificity of the cargo selection and the endocytic route for AMPARs. As endophilin and AP-2 were shown to interact with AMPARs (Lee et al., 2002; Kastning et al., 2007; Zhang et al., 2017), they further strengthen the specificity of the cargo and endocytic molecular machinery.

Endophilin is implicated in AMPAR internalization through its interaction with two other critical signaling molecules required for LTD: Arc/Arg3.1 (Chowdhury et al., 2006) and oligophrenin-1 (Nadif Kasri et al., 2011). Arc/Arg3.1 is rapidly induced by synaptic activation and is required for mGluR-dependent LTD and homeostatic synaptic scaling (Chowdhury et al., 2006; Shepherd et al., 2006). Arc/Arg3.1 forms a protein complex with endophilin 2/3 and dynamin to facilitate AMPAR internalization (Chowdhury et al., 2006). Overexpression of Arc/

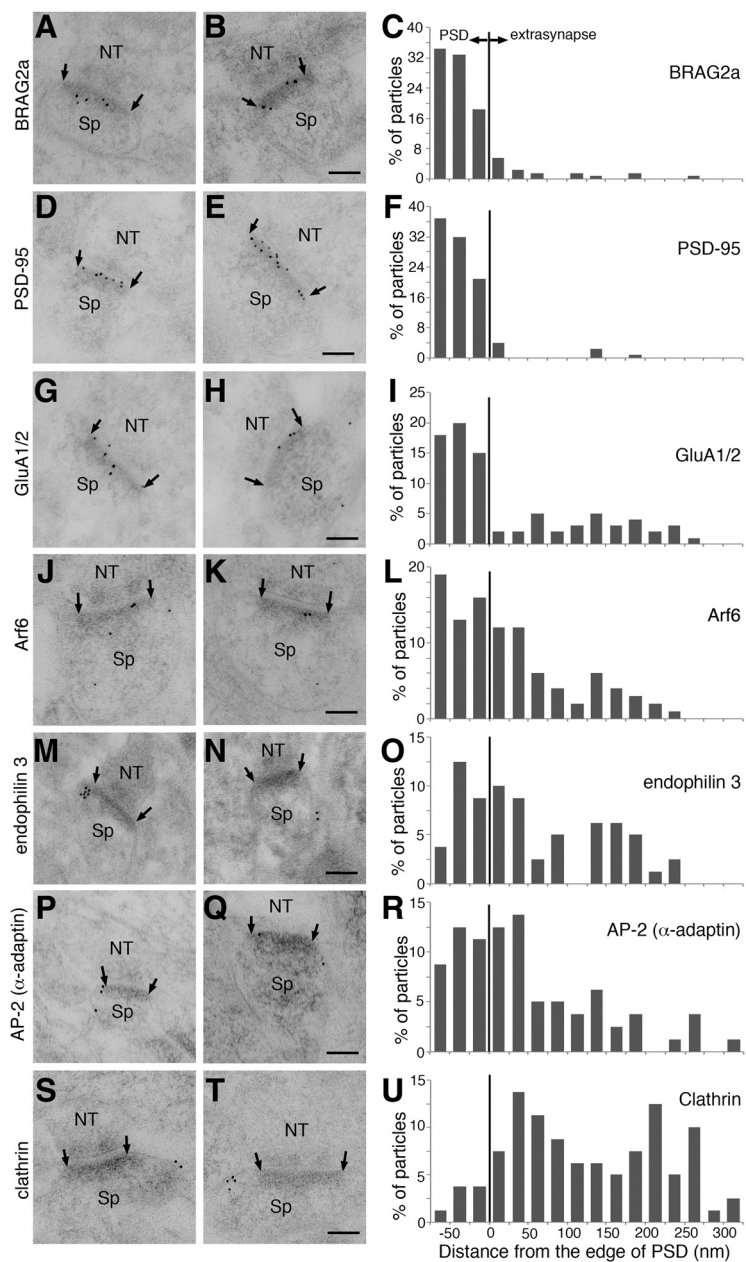


Figure 11. Lateral distribution of BRAG2a, PSD-95, GluA1/2, Arf6, endophilin 3, AP-2, and clathrin along the postsynaptic membrane. *A, B, D, E, G, H, J, K, M, N, P, Q, S, and T*, Representative postembedding immunoelectron microscopic images of the distribution of BRAG2a (*A, B*), PSD-95 (*D, E*), GluA1/2 (*G, H*), Arf6 (*J, K*), endophilin 3 (*M, N*), AP-2/ α -adapitin (*P, Q*), and clathrin (*S, T*) in excitatory asymmetric synapses of the mouse hippocampal CA1 region. *C, F, I, L, O, R, and U*, Histograms showing lateral distribution of immunogold particles for BRAG2a (*C*), PSD-95 (*F*), GluA1/2 (*I*), Arf6 (*L*), endophilin 3 (*O*), AP-2/ α -adapitin (*R*), and clathrin (*U*) along the postsynaptic membrane. The edge of the postsynaptic density (arrows) is defined as 0. The bin size of the histogram is 25 nm, and the synaptic and extrasynaptic sites are shown in the left and right sides, respectively. Scale bars, 100 nm.

Arg3.1, but not its mutants lacking the ability to interact with endophilin or dynamin, decreased the surface expression of GluA1 in cultured hippocampal neurons, whereas neurons from Arc/Arg3.1 knock-out mice exhibited increased surface GluA1 and its endocytosis (Chowdhury et al., 2006). Similarly, oligophrenin-1 is rapidly translated in dendrites in response to mGluR activation, and forms a protein complex with endophilin 2/3 and dynamin, thereby regulating mGluR-dependent AMPAR internalization and LTD (Nadif Kasri et al., 2011). Of note, both BRAG2a and oligophrenin-1 bind to the SH3 domain of endophilin, whereas Arc/Arg3.1 binds to the distinct C-terminal N-BAR

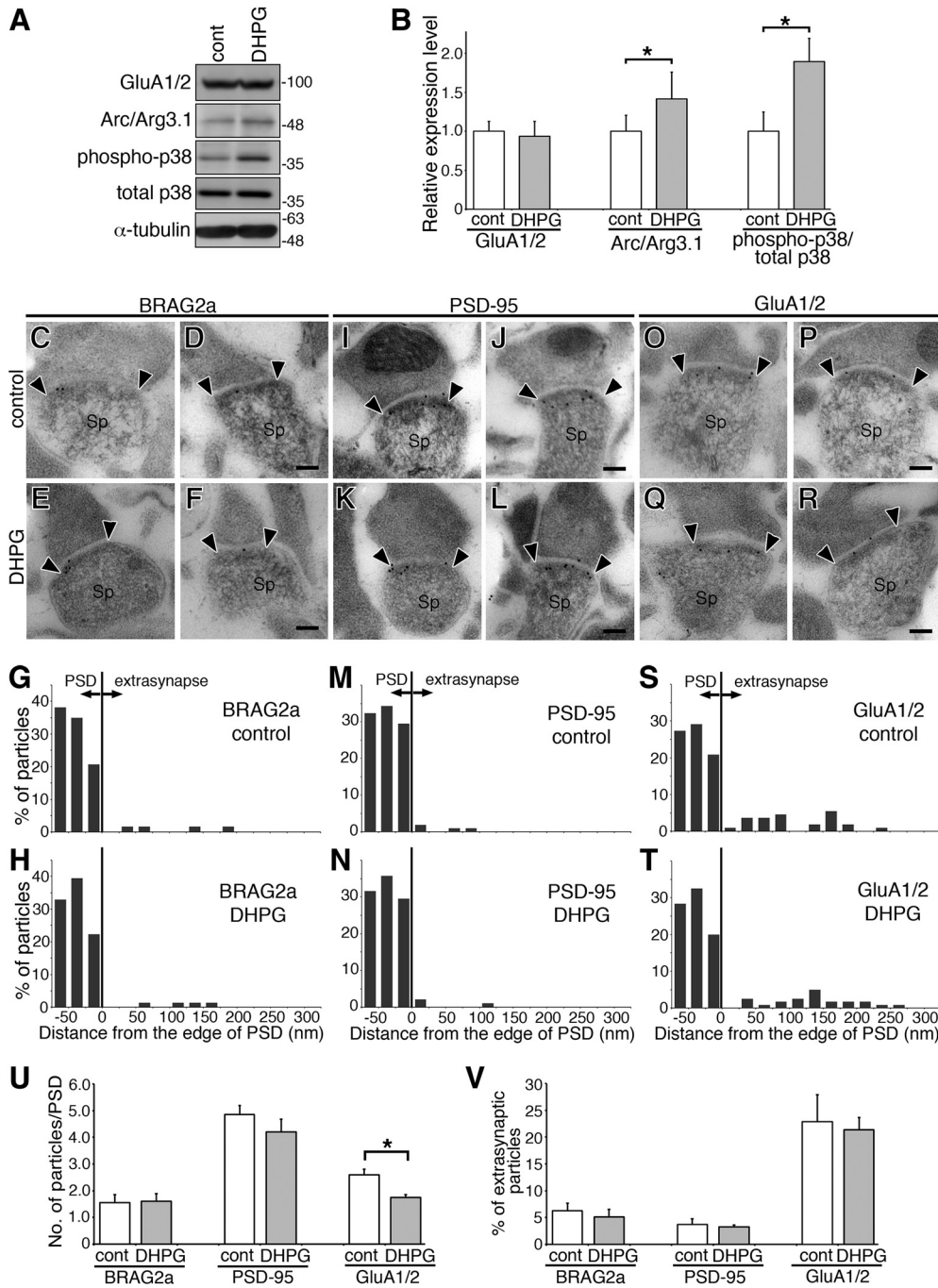


Figure 12. The effect of DHPG treatment on BRAG2a, PSD-95, and GluA1/2 levels in the PSD and extrasynaptic region using acute hippocampal slice cultures. **A, B**, The effect of the DHPG treatment on the expression of GluA1/2 and Arc/Arg3.1, and the phosphorylation of p38 MAPK in acute hippocampal slice cultures. **A**, Representative immunoblots of acute hippocampal slices treated with or without DHPG with anti-GluA1/2, anti-Arc/Arg3.1, anti-phospho-p38 MAPK, anti-p38 MAPK, and anti- α -tubulin antibodies. **B**, Quantification of immunoreactive intensities of GluA1/2, Arc/Arg3.1, and phospho/total p38 MAPKs. Each immunoreactive intensity was normalized by the respective intensity for α -tubulin and expressed as the ratio with the control value. Note that the DHPG treatment induced the significant upregulation of Arc/Arg3.1 and the phosphorylation of p38 MAPK in hippocampal slices. Data for each group were obtained from three culture plates ($n = 3$). These results were confirmed by three independent experiments. **C–T**, Representative postembedding immunoelectron microscopic images (**C–F**, **I–L**, **O–R**) and histograms (**G, H, M, N, S, T**) of the lateral distribution of immunogold particles for BRAG2a (**C–H**), PSD-95 (**I–N**), and GluA1/2 (**O–T**) in axospinous asymmetric synapses in the CA1 stratum radiatum of acute mouse hippocampal slices following 50 μ M DHPG treatment. The edge of the postsynaptic density (arrowheads) is defined as 0. The bin size of the histogram is 25 nm. **U, V**, Quantification of immunogold particles for BRAG2a, PSD-95, and GluA1/2 in the PSD (**U**) and extrasynaptic (**V**) region along the postsynaptic membrane. Values in **U** and **V** are expressed as the average immunogold particle numbers in the PSD of axospinous synapses and the percentage of immunogold particles in the extrasynaptic region in total immunoreactive particles along the postsynaptic membrane, respectively. Note that the DHPG treatment decreased the immunogold particles for GluA1/2 but not BRAG2a or PSD-95 without any changes in the proportion of BRAG2a, PSD-95, or GluA1/2 in the extrasynaptic region. * $p < 0.05$ (t test). Data for each group were obtained from three slices ($n = 3$). These results were confirmed by three independent experiments from different mice. Scale bars, 100 nm.

domain of endophilin. Further studies are needed to elucidate how BRAG2a, Arc/Arg3.1, and oligophrenin-1 cooperatively or distinctively regulate mGluR-dependent AMPAR internalization in hippocampal neurons.

The endocytic zone that mediates activity-dependent AMPAR endocytosis in dendritic spines is positioned on the postsynaptic membrane near the PSD (Lu et al., 2007). On the postsynaptic membrane, the core clathrin-mediated endocytic components, clathrin, AP-2, and dynamin, exhibit preorganized lateral distribution from the PSD to the endocytic zone, depending on the order in which they are involved in the endocytic process, as follows: AP-2 is concentrated closest to the PSD, whereas dynamin is furthest from the PSD (Rácz et al., 2004). The present postembedding immunoelectron microscopy demonstrated that BRAG2a, PSD-95, and AMPARs were highly concentrated in the PSD with a small percentage outside the PSD, whereas Arf6 and endophilin 3 were present in both the PSD and extrasynaptic region. Furthermore, DHPG stimulation of acute hippocampal slices did not induce apparent changes in the ultrastructural distribution of BRAG2a and PSD-95 at postsynapses. Together, these results suggest that BRAG2a is in complex with AMPARs and endophilin 3 only inside the PSD until AMPARs are released from the PSD. Of note, synaptotagmin-3, a calcium sensor protein implicated in membrane trafficking, has recently been shown to regulate activity-dependent AMPAR internalization, LTD, and decay of LTP through the interaction with the tyrosine-rich 3Y motif of GluA2, which BRAG2 also binds to, in the hippocampus (Awasthi et al., 2019). Since GFP-synaptotagmin-3 colocalized well with clathrin-DsRed but not with Homer-myc in transfected neurons, synaptotagmin-3 is considered to function at the endocytic zone rather than PSD. Thus, it is possible to speculate that the interaction of GluA2 with BRAG2a in the PSD may be switched to that with synaptotagmin-3 during its lateral diffusion to the endocytic zone. Alternatively, there also remains a possibility that the BRAG2a–AMPA–endophilin 3 complex may exist only transiently in the extrasynaptic region, thereby escaping the present immunodetection. On the other hand, Arf6 pre-exits widely along the plasma membrane from the PSD to the endocytic zone, which enables Arf6 to regulate sequential endocytic processes from coated pit formation to vesicle scission through multifaceted mechanisms including the activation of lipid-modifying enzymes, such as PIP5K and PLD, and the recruitment of various downstream effectors, such as AP-2 and Nm23-H1, to the postsynaptic membrane.

Accumulating evidence suggests that Arf-GEFs function as a scaffold to link cargo to the endocytic machinery, thereby promoting the activation of Arf at precise timing and location. For example, BRAG2 directly interacts not only with various transmembrane cargo proteins such as EGFR (Morishige et al., 2008), Her2 (Menju et al., 2011), VEGFR2 (Hashimoto et al., 2011), and AMPARs (Scholz et al., 2010), but also with endophilin 3 (this study), clathrin (Moravec et al., 2012), and AP-2 (Moravec et al., 2012). Similarly, EFA6, another Arf6-GEF, interacts with various transmembrane cargo proteins, such as β 2-adrenergic receptors (Macia et al., 2012), TWIK-1 K^+ channels (Decressac et al., 2004), Kir 3.4 K^+ channels (Gong et al., 2007), and telencephalin (Raemaekers et al., 2012), and with endocytic molecular machinery, such as endophilin A1–3, endophilin B1 (Boulakirba et al., 2014), and dynamin (Okada et al., 2015). Therefore, it is tempting to generalize that Arf6-GEFs play a decisive role in the selection of the cargo and endocytic route, as well as in the precise spatiotemporal activation of Arf.

By producing BRAG2 isoform-specific antibodies, we provided immunohistochemical evidence for distinct roles of the following two isoforms in hippocampal neurons: BRAG2a was

selectively localized to the PSD of excitatory synapses, whereas BRAG2b was largely associated with intracellular membrane structures, particularly EEA1-positive vesicles, presumably corresponding to early sorting endosomes, in cell bodies and dendritic shafts. Although both isoforms can interact with AMPARs through the common Sec7 and PH domains, it is reasonable that BRAG2a rather than BRAG2b plays a dominant role in activity-dependent AMPAR endocytosis from the postsynaptic membrane. Under basal conditions, most AMPARs are constitutively internalized and recycled back to the plasma membrane through Arf6-positive recycling endosomes (Zheng et al., 2015). Because BRAG2 was shown to activate not only Arf6, but also the class II Arf members Arf4 and Arf5, which are implicated in vesicular transport from the ER to Golgi and inside the trans-Golgi (Moravec et al., 2012), it is possible to speculate that BRAG2b regulates the intracellular sorting of internalized AMPARs into recycling or degradation pathways.

Finally, hippocampal mGluR-dependent LTD depends on rapid *de novo* protein synthesis in postsynaptic dendrites (Huber et al., 2000), which is regulated by various RNA-binding proteins such as fragile X mental retardation protein (FMRP; Bear et al., 2004). FMRP is the product of the *FMR1* gene, which is responsible for fragile X syndrome (FXS), and functions as a translational suppressor of target mRNAs required for synaptic plasticity. FMR1 knock-out mice exhibit enhanced mGluR-dependent LTD (Huber et al., 2002) and cognitive impairment (Dutch-Belgian Fragile X Consortium, 1994; Santos et al., 2014) because the loss of FMRP exaggerates the translation of its target mRNAs encoding proteins required for LTD, such as Arc/Arg3.1 (Nieme et al., 2012), MAP1b (Hou et al., 2006), and PSD-95 (Muddashetty et al., 2007). Of particular interest, a previous microarray analysis of mRNAs associated with the FMRP ribonucleoprotein complex identified BRAG2 as a possible target mRNA of FMRP (Brown et al., 2001). Although we failed to detect apparent BRAG2 mRNA in hippocampal dendritic fields by *in situ* hybridization or an increase in BRAG2 protein in total lysates of cultured hippocampal neurons stimulated with DHPG by immunoblotting, the possibility that the BRAG2–Arf6 pathway is associated with the pathogenesis of FXS is still worth further investigation.

References

- Alexandropoulos K, Cheng G, Baltimore D (1995) Proline-rich sequences that bind to Src homology 3 domains with individual specificities. *Proc Natl Acad Sci U S A* 92:3110–3114.
- Awasthi A, Ramachandran B, Ahmed S, Benito E, Shinoda Y, Nitzan N, Heukamp A, Rannio S, Martens H, Barth J, Burk K, Wang YT, Fischer A, Dean C (2019) Synaptotagmin-3 drives AMPA receptor endocytosis, depression of synapse strength, and forgetting. *Science* 363:eaav1483.
- Bear MF, Huber KM, Warren ST (2004) The mGluR theory of fragile X mental retardation. *Trends Neurosci* 27:370–377.
- Beaudoin GM 3rd, Lee SH, Singh D, Yuan Y, Ng YG, Reichardt LF, Arikath J (2012) Culturing pyramidal neurons from the early postnatal mouse hippocampus and cortex. *Nat Protoc* 7:1741–1754.
- Blanpied TA, Scott DB, Ehlers MD (2002) Dynamics and regulation of clathrin coats at specialized endocytic zones of dendrites and spines. *Neuron* 36:435–449.
- Bolshakov VY, Carboni L, Cobb MH, Siegelbaum SA, Belardetti F (2000) Dual MAP kinase pathways mediate opposing forms of long-term plasticity at CA3–CA1 synapses. *Nat Neurosci* 3:1107–1112.
- Boulakirba S, Macia E, Partisani M, Lacas-Gervais S, Brau F, Luton F, Franco M (2014) Arf6 exchange factor EFA6 and endophilin directly interact at the plasma membrane to control clathrin-mediated endocytosis. *Proc Natl Acad Sci U S A* 111:9473–9478.

- Brown V, Jin P, Ceman S, Darnell JC, O'Donnell WT, Tenenbaum SA, Jin X, Feng Y, Wilkinson KD, Keene JD, Darnell RB, Warren ST (2001) Microarray identification of FMRP-associated brain mRNAs and altered mRNA translational profiles in fragile X syndrome. *Cell* 107:477–487.
- Carroll RC, Beattie EC, Xia H, Lüscher C, Altschuler Y, Nicoll RA, Malenka RC, von Zastrow M (1999) Dynamically dependent endocytosis of ionotropic glutamate receptors. *Proc Natl Acad Sci U S A* 96:14112–14117.
- Choi S, Ko J, Lee JR, Lee HW, Kim K, Chung HS, Kim H, Kim E (2006) ARF6 and EFA6A regulate the development and maintenance of dendritic spines. *J Neurosci* 26:4811–4819.
- Chowdhury S, Shepherd JD, Okuno H, Lyford G, Petralia RS, Plath N, Kuhl D, Huganir RL, Worley PF (2006) Arc/Arg3.1 interacts with the endocytic machinery to regulate AMPA receptor trafficking. *Neuron* 52:445–459.
- Collingridge GL, Peineau S, Howland JG, Wang YT (2010) Long-term depression in the CNS. *Nat Rev Neurosci* 11:459–473.
- D'Souza RS, Casanova JE (2016) The BRAG/IQSec family of Arf GEFs. *Small GTPases* 7:257–264.
- Decressac S, Franco M, Bendahhou S, Warth R, Knauer S, Barhanin J, Lazdunski M, Lesage F (2004) ARF6-dependent interaction of the TWIK1 K⁺ channel with EFA6, a GDP/GTP exchange factor for ARF6. *EMBO Rep* 5:1171–1175.
- Diering GH, Huganir RL (2018) The AMPA receptor code of synaptic plasticity. *Neuron* 100:314–329.
- Dutch-Belgian Fragile X Consortium (1994) Fmr1 knockout mice: a model to study fragile X mental retardation. *Cell* 78:23–33.
- Elagabani MN, Briševac D, Kintscher M, Pohle J, Köhr G, Schmitz D, Kornau HC (2016) Subunit-selective N-methyl-D-aspartate (NMDA) receptor signaling through brefeldin A-resistant Arf guanine nucleotide exchange factors BRAG1 and BRAG2 during synapse maturation. *J Biol Chem* 291:9105–9118.
- Falace A, Buhler E, Fadda M, Watrin F, Lippello P, Pallesi-Pocachard E, Baldelli P, Benfenati F, Zara F, Represa A, Fassio A, Cardoso C (2014) TBC1D24 regulates neuronal migration and maturation through modulation of the ARF6-dependent pathway. *Proc Natl Acad Sci U S A* 111:2337–2342.
- Fukaya M, Watanabe M (2000) Improved immunohistochemical detection of postsynaptically located PSD-95/SAP90 protein family by protease section pretreatment: a study in the adult mouse brain. *J Comp Neurol* 426:572–586.
- Fukaya M, Kato A, Lovett C, Tonegawa S, Watanabe M (2003) Retention of NMDA receptor NR2 subunits in the lumen of endoplasmic reticulum in targeted NRI1 knockout mice. *Proc Natl Acad Sci U S A* 100:4855–4860.
- Fukaya M, Tsujita M, Yamazaki M, Kushiya E, Abe M, Akashi K, Natsume R, Kano M, Kamiya H, Watanabe M, Sakimura K (2006) Abundant distribution of TARP gamma-8 in synaptic and extrasynaptic surface of hippocampal neurons and its major role in AMPA receptor expression on spines and dendrites. *Eur J Neurosci* 24:2177–2190.
- Fukaya M, Kamata A, Hara Y, Tamaki H, Katsumata O, Ito N, Takeda S, Hata Y, Suzuki T, Watanabe M, Harvey RJ, Sakagami H (2011) SynArfGEF is a guanine nucleotide exchange factor for Arf6 and localizes preferentially at post-synaptic specializations of inhibitory synapses. *J Neurochem* 116:1122–1137.
- Gong Q, Weide M, Huntsman C, Xu Z, Jan LY, Ma D (2007) Identification and characterization of a new class of trafficking motifs for controlling clathrin-independent internalization and recycling. *J Biol Chem* 282:13087–13097.
- Hara Y, Fukaya M, Tamaki H, Sakagami H (2013) Type I phosphatidylinositol 4-phosphate 5-kinase γ is required for neuronal migration in the mouse developing cerebral cortex. *Eur J Neurosci* 38:2659–2671.
- Hara Y, Fukaya M, Hayashi K, Kawauchi T, Nakajima K, Sakagami H (2016) ADP ribosylation factor 6 regulates neuronal migration in the developing cerebral cortex through FIP3/arfophilin-1-dependent endosomal trafficking of N-cadherin. *eNeuro* 3:ENEURO.0148-16.2016.
- Hashimoto A, Hashimoto S, Ando R, Noda K, Ogawa E, Kotani H, Hirose M, Menju T, Morishige M, Manabe T, Toda Y, Ishida S, Sabe H (2011) GEP100-Arf6-AMAP1-cortactin pathway frequently used in cancer invasion is activated by VEGFR2 to promote angiogenesis. *PLoS One* 6:e23359.
- Hernández-Deviez DJ, Casanova JE, Wilson JM (2002) Regulation of dendritic development by the ARF exchange factor ARNO. *Nat Neurosci* 5:623–624.
- Hernández-Deviez DJ, Roth MG, Casanova JE, Wilson JM (2004) ARNO and ARF6 regulate axonal elongation and branching through downstream activation of phosphatidylinositol 4-phosphate 5-kinase alpha. *Mol Biol Cell* 15:111–120.
- Hou L, Antion MD, Hu D, Spencer CM, Paylor R, Klann E (2006) Dynamic translational and proteasomal regulation of fragile X mental retardation protein controls mGluR-dependent long-term depression. *Neuron* 51:441–454.
- Huber KM, Kayser MS, Bear MF (2000) Role for rapid dendritic protein synthesis in hippocampal mGluR-dependent long-term depression. *Science* 288:1254–1257.
- Huber KM, Gallagher SM, Warren ST, Bear MF (2002) Altered synaptic synaptic plasticity in a mouse model of fragile X mental retardation. *Proc Natl Acad Sci U S A* 99:7746–7750.
- Jordan BA, Fernholz BD, Boussac M, Xu C, Grigorean G, Ziff EB, Neubert TA (2004) Identification and verification of novel rodent postsynaptic density proteins. *Mol Cell Proteomics* 3:857–871.
- Kastning K, Kukhtina V, Kittler JT, Chen G, Pechstein A, Enders S, Lee SH, Sheng M, Yan Z, Haucke V (2007) Molecular determinants for the interaction between AMPA receptors and the clathrin adaptor complex AP-2. *Proc Natl Acad Sci U S A* 104:2991–2996.
- Kim Y, Lee SE, Park J, Kim M, Lee B, Hwang D, Chang S (2015) ADP-ribosylation factor 6 (ARF6) bidirectionally regulates dendritic spine formation depending on neuronal maturation and activity. *J Biol Chem* 290:7323–7335.
- Lee SH, Liu L, Wang YT, Sheng M (2002) Clathrin adaptor AP2 and NSF interact with overlapping sites of GluR2 and play distinct roles in AMPA receptor trafficking and hippocampal LTD. *Neuron* 36:661–674.
- Lu J, Helton TD, Blanpied TA, Rácz B, Newpher TM, Weinberg RJ, Ehlers MD (2007) Postsynaptic positioning of endocytic zones and AMPA receptor cycling by physical coupling of dynamin-3 to Homer. *Neuron* 55:874–889.
- Macia E, Partisani M, Paleotti O, Luton F, Franco M (2012) Arf6 negatively controls the rapid recycling of the β 2 adrenergic receptor. *J Cell Sci* 125:4026–4035.
- Malinow R, Malenka RC (2002) AMPA receptor trafficking and synaptic plasticity. *Annu Rev Neurosci* 25:103–126.
- Man HY, Lin JW, Ju WH, Ahmadian G, Liu L, Becker LE, Sheng M, Wang YT (2000) Regulation of AMPA receptor-mediated synaptic transmission by clathrin-dependent receptor internalization. *Neuron* 25:649–662.
- Menju T, Hashimoto S, Hashimoto A, Otsuka Y, Handa H, Ogawa E, Toda Y, Wada H, Date H, Sabe H (2011) Engagement of overexpressed Her2 with GEP100 induces autonomous invasive activities and provides a biomarker for metastases of lung adenocarcinoma. *PLoS One* 6:e25301.
- Miyazaki H, Yamazaki M, Watanabe H, Maehama T, Yokozeki T, Kanaho Y (2005) The small GTPase ADP-ribosylation factor 6 negatively regulates dendritic spine formation. *FEBS Lett* 579:6834–6838.
- Moravec R, Conger KK, D'Souza R, Allison AB, Casanova JE (2012) BRAG2/GEP100/IQSec1 interacts with clathrin and regulates α 5 β 1 integrin endocytosis through activation of ADP ribosylation factor 5 (Arf5). *J Biol Chem* 287:31138–31147.
- Morishige M, Hashimoto S, Ogawa E, Toda Y, Kotani H, Hirose M, Wei S, Hashimoto A, Yamada A, Yano H, Mazaki Y, Kodama H, Nio Y, Manabe T, Wada H, Kobayashi H, Sabe H (2008) GEP100 links epidermal growth factor receptor signalling to Arf6 activation to induce breast cancer invasion. *Nat Cell Biol* 10:85–92.
- Muddashetty RS, Kelić S, Gross C, Xu M, Bassell GJ (2007) Dysregulated metabotropic glutamate receptor-dependent translation of AMPA receptor and postsynaptic density-95 mRNAs at synapses in a mouse model of fragile X syndrome. *J Neurosci* 27:5338–5348.
- Nadif Kasri N, Nakano-Kobayashi A, Van Aelst L (2011) Rapid synthesis of the X-linked mental retardation protein OPHN1 mediates mGluR-dependent LTD through interaction with the endocytic machinery. *Neuron* 72:300–315.
- Nakayama K, Takatsu H (2005) Analysis of Arf interaction with GGAs in vitro and in vivo. *Methods Enzymol* 404:367–377.
- Niere F, Wilkerson JR, Huber KM (2012) Evidence for a fragile X mental retardation protein-mediated translational switch in metabotropic glutamate receptor-triggered Arc translation and long-term depression. *J Neurosci* 32:5924–5936.
- Okada R, Yamauchi Y, Hongu T, Funakoshi Y, Ohbayashi N, Hasegawa H, Kanaho Y (2015) Activation of the small G protein Arf6 by Dynamin2

- through guanine nucleotide exchange factors in endocytosis. *Sci Rep* 5:14919.
- Peng J, Kim MJ, Cheng D, Duong DM, Gygi SP, Sheng M (2004) Semiquantitative proteomic analysis of rat forebrain postsynaptic density fractions by mass spectrometry. *J Biol Chem* 279:21003–21011.
- Rác B, Blanpied TA, Ehlers MD, Weinberg RJ (2004) Lateral organization of endocytic machinery in dendritic spines. *Nat Neurosci* 7:917–918.
- Raemaekers T, Peric A, Baatsen P, Sannerud R, Declerck I, Baert V, Michiels C, Annaert W (2012) ARF6-mediated endosomal transport of Telencephalin affects dendritic filopodia-to-spine maturation. *EMBO J* 31:3252–3269.
- Ringstad N, Nemoto Y, De Camilli P (1997) The SH3p4/Sh3p8/SH3p13 protein family: binding partners for synaptojanin and dynamin via a Grb2-like Src homology 3 domain. *Proc Natl Acad Sci U S A* 94:8569–8574.
- Ringstad N, Gad H, Löw P, Di Paolo G, Brodin L, Shupliakov O, De Camilli P (1999) Endophilin/SH3p4 is required for the transition from early to late stages in clathrin-mediated synaptic vesicle endocytosis. *Neuron* 24:143–154.
- Sakagami H, Kamata A, Fukunaga K, Kondo H (2005) Functional assay of EFA6A, a guanine nucleotide exchange factor for ADP-ribosylation factor 6 (ARF6), in dendritic formation of hippocampal neurons. *Methods Enzymol* 404:232–242.
- Sakagami H, Suzuki H, Kamata A, Owada Y, Fukunaga K, Mayanagi H, Kondo H (2006) Distinct spatiotemporal expression of EFA6D, a guanine nucleotide exchange factor for ARF6, among the EFA6 family in mouse brain. *Brain Res* 1093:1–11.
- Sakagami H, Sanda M, Fukaya M, Miyazaki T, Sukegawa J, Yanagisawa T, Suzuki T, Fukunaga K, Watanabe M, Kondo H (2008) IQ-ArfGEF/BRAG1 is a guanine nucleotide exchange factor for Arf6 that interacts with PSD-95 at postsynaptic density of excitatory synapses. *Neurosci Res* 60:199–212.
- Sakagami H, Katsumata O, Hara Y, Tamaki H, Watanabe M, Harvey RJ, Fukaya M (2013) Distinct synaptic localization patterns of brefeldin A-resistant guanine nucleotide exchange factors BRAG2 and BRAG3 in the mouse retina. *J Comp Neurol* 521:860–876.
- Sakagami H, Katsumata O, Hara Y, Sasaoka T, Fukaya M (2017) BRAG2a, a guanine nucleotide exchange factor for Arf6, is a component of the dystrophin-associated glycoprotein complex at the photoreceptor terminal. *Invest Ophthalmol Vis Sci* 58:3795–3803.
- Santos AR, Kanellopoulos AK, Bagni C (2014) Learning and behavioral deficits associated with the absence of the fragile X mental retardation protein: what a fly and mouse model can teach us. *Learn Mem* 21:543–555.
- Scholz R, Berberich S, Rathgeber L, Kollekler A, Köhr G, Kornau HC (2010) AMPA receptor signaling through BRAG2 and Arf6 critical for long-term synaptic depression. *Neuron* 66:768–780.
- Schuske KR, Richmond JE, Matthies DS, Davis WS, Runz S, Rube DA, van der Blik AM, Jorgensen EM (2003) Endophilin is required for synaptic vesicle endocytosis by localizing synaptojanin. *Neuron* 40:749–762.
- Sheng M, Lee SH (2001) AMPA receptor trafficking and the control of synaptic transmission. *Cell* 105:825–828.
- Shepherd JD, Rumbaugh G, Wu J, Chowdhury S, Plath N, Kuhl D, Huganir RL, Worley PF (2006) Arc/Arg3.1 mediates homeostatic synaptic scaling of AMPA receptors. *Neuron* 52:475–484.
- Someya A, Sata M, Takeda K, Pacheco-Rodriguez G, Ferrans VJ, Moss J, Vaughan M (2001) ARF-GEP(100), a guanine nucleotide-exchange protein for ADP-ribosylation factor 6. *Proc Natl Acad Sci U S A* 98:2413–2418.
- Tagliatti E, Fadda M, Falace A, Benfenati F, Fassio A (2016) Arf6 regulates the cycling and the readily releasable pool of synaptic vesicles at hippocampal synapse. *eLife* 5:e10116.
- Watanabe M, Fukaya M, Sakimura K, Manabe T, Mishina M, Inoue Y (1998) Selective scarcity of NMDA receptor channel subunits in the stratum lucidum (mossy fibre-recipient layer) of the mouse hippocampal CA3 subfield. *Eur J Neurosci* 10:478–487.
- Wang MW, Pfeiffer BE, Nosyreva ED, Ronesi JA, Huber KM (2008) Rapid translation of Arc/Arg3.1 selectively mediates mGluR-dependent LTD through persistent increases in AMPAR endocytosis rate. *Neuron* 59:84–97.
- Yazaki Y, Hara Y, Tamaki H, Fukaya M, Sakagami H (2014) Endosomal localization of FIP3/Arfophilin-1 and its involvement in dendritic formation of mouse hippocampal neurons. *Brain Res* 1557:55–65.
- Zhang J, Yin Y, Ji Z, Cai Z, Zhao B, Li J, Tan M, Guo G (2017) Endophilin2 interacts with GluA1 to mediate AMPA receptor endocytosis induced by oligomeric amyloid- β . *Neural Plast* 2017:8197085.
- Zheng N, Jeyifous O, Munro C, Montgomery JM, Green WN (2015) Synaptic activity regulates AMPA receptor trafficking through different recycling pathways. *eLife* 4:e06878.